JOURNAL OF PETROLOGY | VOLUME 45 | NUMBER 11 | PAGES 2261–2286 | 2004 | doi:10.1093/petrology/egh055

The Effect of Cr_2O_3 on the Partial Melting of Spinel Lherzolite in the System CaO–MgO–Al_2O_3–SiO_2–Cr_2O_3 at 1·1 GPa

XI LIU[1] AND HUGH ST. C. O'NEILL*

RESEARCH SCHOOL OF EARTH SCIENCES, AUSTRALIAN NATIONAL UNIVERSITY, CANBERRA, A.C.T. 0200, AUSTRALIA

RECEIVED AUGUST 4, 2003; ACCEPTED JUNE 30, 2004
ADVANCE ACCESS PUBLICATION SEPTEMBER 9, 2004

Chromium as Cr^{3+} substitutes for octahedrally coordinated Al in upper-mantle minerals, thereby reducing the activity of Al_2O_3 in the system and hence the concentration of Al_2O_3 in partial melts. The effect of Cr_2O_3 on melt compositions multiply saturated with the spinel lherzolite phase assemblage has been quantified in the system CaO–MgO–Al_2O_3–SiO_2–Cr_2O_3 at 1·1 GPa as a function of 100 Cr/(Cr + Al) in the spinel ($Cr\#_{sp}$). The decrease of Al_2O_3 in the melt with increasing $Cr\#_{sp}$ is accompanied by increasing MgO and SiO_2, whereas CaO remains almost constant. Consequently, the CaO/Al_2O_3 ratio of the melt increases with $Cr\#_{sp}$, and the melt becomes richer in normative diopside, hypersthene and quartz. The effect may explain certain mantle melts with unusually high CaO/Al_2O_3 ratios. The concentration of Cr_2O_3 in the melt remains low even at high $Cr\#_{sp}$, which means that the strong effect of Cr_2O_3 on partial melting equilibria is not readily apparent from its concentration in the melt itself. The existence of a highly refractory major component such as Cr_2O_3 nullifies simplified conclusions from the 'inverse approach' in the experimental study of basalt petrogenesis, as there is insufficient information in the composition of the partial melt to reconstruct the conditions of melting.

KEY WORDS: *basalt petrogenesis; partial melting; reversal experiment; spinel lherzolite; system CMAS–Cr_2O_3; CaO/Al_2O_3 of melt; effect of Cr_2O_3*

INTRODUCTION

Most, if not all, basaltic magmas are produced by the partial melting of mantle peridotite. From a chemical perspective, partial melting involves a reaction between the melt and the residual solid phases; however, igneous petrologists have traditionally taken a magmacentric view of the process, because it is the magma that emerges at the Earth's surface for examination. This perspective has encouraged a common assumption in basalt petrogenetic studies that all the necessary chemical information about the partial melting process is contained in the magma composition. Such an assumption would not be valid if there were a component in the system that was completely absent from the magma but occurred only in the residue—that is, a completely refractory component with bulk melt/solid distribution coefficient of zero.

A completely refractory component may only be a hypothetical construct, but Cr_2O_3 comes close. Its abundance in magmas is only in the minor to trace element range, thus its importance in determining the chemical composition of basaltic magmas may not be obvious from the chemistry of the magmas themselves. However, Cr_2O_3 substitutes for Al_2O_3 in the solid phases of the mantle, reducing the activity of Al_2O_3 in the system, and hence in derived partial melts.

This study aims to evaluate the effect of Cr on the partial melting of mantle peridotite, by systematic additions of Cr_2O_3 to the model system CaO–MgO–Al_2O_3–SiO_2 (CMAS). The CMAS system is the simplest system in which four phases (olivine, orthopyroxene, clinopyroxene and an aluminous phase, plagioclase, spinel or garnet, depending on pressure), as typically developed in fertile upper-mantle peridotite compositions, are stable. It therefore provides an excellent starting point from which to understand mantle phase equilibria.

Partial melting of a four-phase assemblage in the system CMAS is isobarically invariant, and the chemical

*Corresponding author. Telephone: (+61) 2 6125 5159. Fax: (+61) 2 6125 5989. E-mail: hugh.oneill@anu.edu.au
[1]Present address: Geodynamics Research Center, Ehime University, Matsuyama 790-8577, Japan.

potentials of all four components (CaO, MgO, Al_2O_3 and SiO_2) of the melt are completely defined, for example, by the following reactions:

$$\underset{\text{Melt}}{\text{CaO}} + 1{\cdot}5\underset{\text{Opx}}{\text{Mg}_2\text{Si}_2\text{O}_6} = \underset{\text{Cpx}}{\text{CaMgSi}_2\text{O}_6} + \underset{\text{Ol}}{\text{Mg}_2\text{SiO}_4} \quad (1)$$

$$\underset{\text{Melt}}{\text{MgO}} + 0{\cdot}5\underset{\text{Opx}}{\text{Mg}_2\text{Si}_2\text{O}_6} = \underset{\text{Ol}}{\text{Mg}_2\text{SiO}_4} \quad (2)$$

$$\underset{\text{Melt}}{\text{SiO}_2} + \underset{\text{Ol}}{\text{Mg}_2\text{SiO}_4} = \underset{\text{Opx}}{\text{Mg}_2\text{Si}_2\text{O}_6} \quad (3)$$

and in the spinel stability field:

$$\underset{\text{Melt}}{\text{AlO}_{1{\cdot}5}} + 0{\cdot}5\underset{\text{Ol}}{\text{Mg}_2\text{SiO}_4} = 0{\cdot}5\underset{\text{Sp}}{\text{MgAl}_2\text{O}_4} + 0{\cdot}25\underset{\text{Opx}}{\text{Mg}_2\text{Si}_2\text{O}_6}. \quad (4)$$

Reaction (4) encapsulates the pivotal point of this study. As Cr_2O_3 substitutes for Al_2O_3 in Sp, the activity of Al_2O_3 in the melt is correspondingly reduced. Because molar $100Cr/(Cr + Al)$ in the spinels (hereafter, $Cr\#_{sp}$) in mantle peridotites can vary from 10 to 80 [e.g. with depletion by previous melt extraction; Dick & Bullen (1984) and Barnes & Roeder (2001)], the effect is very large. The other melt components (CaO, MgO and SiO_2) do not depend directly on the activities of aluminous components [reactions (1)–(3)], hence their activities remain nearly constant as Cr_2O_3 is varied.

It is important to note that the Cr_2O_3 effect does not depend on the presence of spinel, although there is a relationship with the pressure regime. For example, the presence of plagioclase, the aluminous phase in lherzolitic compositions at lower pressures, would buffer the activity of Al_2O_3, ostensibly independently of Cr_2O_3, according to the reaction

$$\underset{\text{Melt}}{\text{AlO}_{1{\cdot}5}} + 0{\cdot}5\underset{\text{Cpx}}{\text{CaMgSi}_2\text{O}_6} + 0{\cdot}25\underset{\text{Opx}}{\text{Mg}_2\text{Si}_2\text{O}_6} = 0{\cdot}5\underset{\text{Plag}}{\text{CaAl}_2\text{Si}_2\text{O}_8} + \underset{\text{Ol}}{\text{Mg}_2\text{SiO}_4}. \quad (5)$$

However, plagioclase is itself suppressed by high Cr_2O_3 activity, owing to the stability of Cr-rich spinel, as may be seen from the reaction

$$\underset{\text{Plag}}{\text{CaAl}_2\text{Si}_2\text{O}_8} + \underset{\text{Ol}}{\text{Mg}_2\text{SiO}_4} = \underset{\text{Sp}}{\text{MgAl}_2\text{O}_4} + \underset{\text{Cpx}}{\text{CaMgSi}_2\text{O}_6} + \underset{\text{Opx}}{\text{Mg}_2\text{Si}_2\text{O}_6}. \quad (6)$$

Thus the constant activity of Al_2O_3 implied by reaction (5) is possible only over a limited range of Al_2O_3/Cr_2O_3 ratios, this range expanding with decreasing pressure according to reaction (6). It is therefore instructive to consider the Cr_2O_3 effect from the point of view of the Al_2O_3 content in pyroxenes. The reaction controlling Al_2O_3 in the melt could equally validly be written

$$\underset{\text{Melt}}{\text{AlO}_{1{\cdot}5}} + 0{\cdot}25\underset{\text{Opx}}{\text{Mg}_2\text{Si}_2\text{O}_6} = 0{\cdot}5\underset{\text{Opx}}{\text{MgAl}_2\text{SiO}_6}. \quad (7)$$

Cr_2O_3 substituting for Al_2O_3 in orthopyroxene diminishes the activity of the $MgAl_2SiO_6$ component (see Klemme & O'Neill, 2000), reducing the Al_2O_3 in the melt in a similar way to reaction (4). Reaction (7) becomes equivalent to reaction (4) at spinel saturation, the two reactions being linked by the reaction

$$\underset{\text{Sp}}{\text{MgAl}_2\text{O}_4} + \underset{\text{Opx}}{\text{Mg}_2\text{Si}_2\text{O}_6} = \underset{\text{Opx}}{\text{MgAl}_2\text{SiO}_6} + \underset{\text{Ol}}{\text{Mg}_2\text{SiO}_4}. \quad (8)$$

We have elected to study the Cr_2O_3 effect at spinel saturation, as the thermodynamic properties of the melt are most rigorously constrained when it is multiply saturated in all four solid phases, although we emphasize again that the phenomenon is not dependent on the presence of spinel [reaction (7)]. Nor is the Cr_2O_3 effect in any way limited to the low degrees of partial melting associated with multiple saturation; rather, the effect should become more pronounced with increasing melt fraction, as the Cr_2O_3/Al_2O_3 ratio in the residual solid phases increases.

Previous work on the influence of Cr_2O_3 on the phase relationships of the CMAS system at supersolidus conditions is limited. Irvine (1977) showed that Sp could be stabilized in all melts in the join Fo–Di–An–Qz by adding a small amount of Cr_2O_3 to the CMAS system. Libourel (1991) found that the addition of Cr_2O_3 to the CMAS system stabilizes spinel in equilibrium with plagioclase lherzolite at 1 bar; he located the isobaric invariant point at which Ol + Opx + Cpx + Pl + Sp coexist with melt, which contained only 0·15 wt % Cr_2O_3 at 1249 ± 2°C. Libourel's study appeared only as a conference abstract, and we are not aware of any other studies at higher pressure.

The effect of Cr_2O_3 on subsolidus equilibria is better known. O'Neill (1981) and Nickel (1986) demonstrated the importance of Cr_2O_3 on the transition between garnet lherzolite and spinel lherzolite. Klemme & O'Neill (2000) studied the equilibrium between Opx and Sp coexisting with Fo in the system MAS–Cr_2O_3; these phase relations are the key to understanding the controls on the activity of Al_2O_3 [reactions (4) and (7)]. Li *et al.* (1995) studied the system MgO–SiO_2–Cr–O in equilibrium with metallic Cr, in which most of the Cr occurs as Cr^{2+}. They showed that Cr^{2+}, which behaves geochemically very unlike Cr^{3+}, readily substitutes for Mg in Ol and Opx solid solutions.

Table 1: Compositions of starting materials used in this study

	Sandwiching part					Sandwiched part		
	SEM05-1	SEM04-1	SEM01-1	SEM03-1	SEM06-1	SEM01-4-1	SEM01-4-2	SEM01-5
SiO_2	37·02	37·86	37·90	38·77	38·81	52·39	52·39	51·34
Al_2O_3	17·49	12·76	9·73	5·90	3·61	14·66	14·66	14·37
Cr_2O_3	5·64	9·59	12·40	14·86	17·18	0·48	0·48	0·47
MgO	34·40	34·38	34·75	34·94	34·88	17·15	17·15	16·80
CaO	5·45	5·40	5·21	5·53	5·53	14·31	14·31	14·02
K_2O	0·00	0·00	0·00	0·00	0·00	1·00	1·00	3·00
Cr# (by mole)	17·8	33·5	46·1	62·8	76·1	2·1	2·1	2·1
Internal buffer	No	No	Yes	No	No	Yes	No	No

Cr# is the ratio of Cr/(Cr + Al). Internal buffer is the buffer RuO_2 (11·3 wt % in SEM01-1 and 8·47 wt % in SEM01-4-1). The ratio of Ol, Sp, Opx and Cpx in SEM05-1, SEM04-1, SEM03-1 and SEM06-1 approximates 1:1:1:1. The compositions of these solid phases came from Walter & Presnall (1994) or from our preliminary experiments.

EXPERIMENTAL

Experimental strategy

Experimentally, the aim of this study is to determine how Cr_2O_3 affects the compositions of the melt and the solid phases, as well as the partial melting temperature, for the spinel lherzolite phase assemblage in the system CMAS–Cr_2O_3. A pressure of 1·1 GPa was chosen as the spinel lherzolite phase assemblage is stable at this pressure, and we could build on previous work in the system CMAS (Presnall *et al.*, 1979; Walter & Presnall, 1994; Liu & O'Neill, 2004). This pressure has been advocated by some workers as close to the average pressure for the production of mid-ocean ridge basalts (MORBs), both from experimental constraints (Presnall *et al.*, 1979, 2002; Sen, 1982; Presnall & Hoover, 1984, 1987) and from seismic observations (Melt Seismic Team, 1998; Dunn & Forsyth, 2001).

There are five components in the system CMAS–Cr_2O_3; if the presence of five phases at the solidus is stipulated (Ol + Sp + Opx + Cpx + Melt), the system has one degree of freedom at constant pressure, and therefore one additional variable is required to describe the system completely. In this study, the parameter $Cr\#_{sp}$, defined as molar 100Cr/(Cr + Al) in spinel, is used as the necessary variable.

As the system is isobarically univariant in the presence of four crystalline phases, it should be possible, at least theoretically, to observe the full spinel lherzolite phase assemblage coexisting with melt over a finite temperature interval above the solidus. However, preliminary experiments showed that this temperature interval was only ~10°C for bulk compositions that give reasonable amounts of all phases; this is close to the temperature resolution of the experiments (~± 5°C). We therefore adopted the strategy of deliberately introducing an extra component into the system, to increase the temperature interval over which Ol + Sp + Opx + Cpx + Melt could coexist. We chose K_2O, as this component enters only the melt. Previously we have found that adding K_2O expands the temperature interval over which Ol + Sp + Opx + Cpx + Melt is stable to ~60° in the system CMAS–K_2O (Liu & O'Neill, 2004). The composition of the melt in the K_2O-free system is then obtained by extrapolating the data empirically to zero K_2O. This procedure has been thoroughly tested for the system CMAS–K_2O (Liu & O'Neill, 2004), and produces results that agree well with previous work.

An experimental problem in many peridotite partial-melting studies is crystallization from the melt during quenching. In the system CMAS–Cr_2O_3, both the temperature of the solidus rises and the amount of MgO in the melt increases with increasing $Cr\#_{sp}$, exacerbating the problem. In our first attempts at experiments at high-Cr_2O_3 compositions in the system CMAS–Cr_2O_3, quench Ol was ubiquitous, and melt compositions could not be confidently determined. This problem is also ameliorated by the addition of K_2O, both by lowering the solidus temperature and by making the melt composition less picritic. The 'K_2O method', in conjunction with the 'sandwich method', can produce large pools of melt in run products, in which the effects of quench modification are effectively eliminated except at $Cr\#_{sp} = 100$, at which quench modification is so severe that we were unable to gain any useful results.

Starting materials

Table 1 summarizes the starting materials used in this study. Two types of starting materials were prepared.

Table 2: Experimental conditions and summary of results

Run no.	Starting material	T (°C)	t (h)	Phase observed	K_2O-melt	T-1	T-2	T-3	T-4	Notes
Experiment Set 5 [bulk Cr/(Cr + Al) = 0·13, Cr#$_{sp}$ ~20]										
C-1550	SEM05-1 + SEM01-5	1360	51·5	Ol + Sp + Opx + Melt	1·61	—	—	—	—	
C-1527	SEM05-1 + SEM01-4-2	1350	53	Ol + Sp + Opx + Cpx + Melt	0·85	1308	1352	1315	1379	
D-82	SEM05-1 + SEM01-5	1340	50	Ol + Sp + Opx + Cpx + Melt	2·62	1305	1347	1290	1331	
C-1511	SEM05-1 + SEM01-5	1330	92	Ol + Sp + Opx + Cpx + Melt	4·08	1306	1350	1286	1296	zoned Sp and Cpx*
Experiment Set 4 [bulk Cr/(Cr + Al) = 0·23, Cr#$_{sp}$ ~40]										
C-1499	SEM04-1 + SEM01-5	1360	70	Ol + Sp + Opx + Cpx + Melt	1·80	1357	1388	1339	1424	
C-1481	SEM04-1 + SEM01-5	1350	71	Ol + Sp + Opx + Cpx + Melt	3·06	1405	1428	1347	1397	
C-1478	SEM04-1 + SEM01-5	1340	70	Ol + Sp + Opx + Cpx + Melt	5·76	1345	1381	1302	1375	zoned Sp and Cpx
C-1480	SEM04-1 + SEM01-5	1320	74	Ol + Sp + Opx + Cpx + Melt†	—	1340	1378	1307	—	zoned Sp and Cpx
Experiment Set 1 [bulk Cr/(Cr + Al) = 0·29, Cr#$_{sp}$ ~50]										
C-1459	SEM01-1 + SEM01-5	1360	70	Ol + Sp + Opx + Melt	1·77	—	—	—	—	
C-1414	SEM01-1 + SEM01-4-1	1360	72	Ol + Sp + Opx + Cpx + Melt	0·87	1358	1395	1362	1430	
C-1472	SEM01-1 + SEM01-5	1350	70	Ol + Sp + Opx + Cpx + Melt	2·54	1372	1400	1327	1410	
C-1449	SEM01-1 + SEM01-5	1340	72	Ol + Sp + Opx + Cpx + Melt	3·26	1352	1389	1319	1392	zoned Sp and Cpx
C-1469	SEM01-1 + SEM01-5	1330	72	Ol + Sp + Opx + Cpx + Melt	4·26	1351	1390	1311	1326	zoned Sp and Cpx
Experiment Set 3 [bulk Cr/(Cr + Al) = 0·34, Cr#$_{sp}$ ~60]										
C-1489	SEM03-1 + SEM01-4-2	1360	74	Ol + Sp + Opx + Cpx + Melt	1·19	1454	1457	1377	1451	
C-1463	SEM03-1 + SEM01-5	1350	74	Ol + Sp + Opx + Cpx + Melt	2·97	1390	1419	1358	1426	zoned Sp
C-1476	SEM03-1 + SEM01-5	1330	72	Ol + Sp + Opx + Cpx + Melt	5·11	1372	1404	1358	1407	zoned Sp and Cpx
Experiment Set 6 [bulk Cr/(Cr + Al) = 0·42, Cr#$_{sp}$ ~75]										
C-1516	SEM06-1 + SEM01-5	1380	52	Ol + Sp + Opx + Cpx + Melt	2·07	1561	1504	1396	1477	
C-1512	SEM06-1 + SEM01-5	1370	56	Ol + Sp + Opx + Cpx + Melt	3·02	1486	1480	1381	1456	zoned Sp and Cpx
C-1515	SEM06-1 + SEM01-5	1360	68·5	Ol + Sp + Opx + Cpx + Melt	4·01	1448	1458	1362	1444	zoned Sp and Cpx

The 'sandwich' configuration was used in all experiments. Each 'set' of experiments is identified by the bulk molar Cr/(Cr + Al) in the starting composition, and the approximate Cr#$_{sp}$ in the run products. An internal oxygen buffer of Ru + RuO_2 was used in Experiment Set 1. T-1 to T-4 are the temperatures calculated using the following geothermometers: T-1, Nickel *et al*. (1985); T-2, the Opx—Cpx geothermometer of Brey & Kohler [1990; equation (9)]; T-3, the Ca-in-Opx geothermometer of Brey & Kohler [1990; equation (10)]; T-4, Ford *et al*. (1983).
*Zoned Sp and Cpx: compositional zoning in Sp and/or Cpx crystallizing in the 'sandwiched' layer, which was originally glass (see Fig. 2). Reported analyses in Table 3 are from the 'sandwiching' layers.
†Melt: confirmed but cannot be properly analysed.

Crystalline mixtures SEM05-1, SEM04-1, SEM01-1, SEM03-1 and SEM06-1 were made with a 5/8 inch piston-cylinder press by crystallizing the decarbonated oxide mixes at 1300°C, 1·1 GPa (i.e. subsolidus) and 48 h in a 3·5 mm diameter Pt capsule. This produced fine-grained but well-crystallized assemblages, in which the average compositions of the pyroxenes should be approximately appropriate to the P, T conditions of this study. Glasses SEM01-4-1, SEM01-4-2 and SEM01-5 were synthesized at 1400°C, 1 bar and 20 min, and then quenched to glass. High-purity oxides (SiO_2, Al_2O_3, Cr_2O_3 and MgO) and carbonates ($CaCO_3$ and K_2CO_3) were used. All mixtures were checked for bulk composition with the electron microprobe (Ware, 1991). To control experimental oxygen fugacity at high values, RuO_2 was mixed into SEM05-1 and SEM01-4-1 (O'Neill & Nell, 1997).

Capsule configuration and cell arrangement

All experiments were made in a conventional $\frac{1}{2}$ inch piston-cylinder apparatus with a NaCl–Pyrex assembly, using sealed Pt capsules and the so-called 'sandwich technique', in which a layer of the anticipated melt composition (powdered glass starting material) is placed between two layers of an appropriate crystalline assemblage of Ol + Opx + Cpx + Sp. The proportion of the melt part to the crystalline part was adjusted to keep the Cr/(Cr + Al) ratio of the bulk compositions in each set of experiments constant (Table 2). Full experimental details have been given by Liu (2003) and Liu & O'Neill (2004).

To prevent reduction of Cr^{3+} to Cr^{2+}, it is critically important to eliminate any diffusion of H_2 into the capsule. Such a precaution also ensures that the experiments are not contaminated by water. Therefore, as in our previous study (Liu & O'Neill, 2004) the Pt capsule was surrounded by a sleeve of Fe_2O_3 to act as a H_2 getter.

Run products were analysed on a JEOL 6400 scanning electron microprobe in energy dispersive mode (EDS) at the Electron Microprobe Unit (EMU) at ANU. Beam current was 1 nA, accelerating voltage was 15 keV and the ZAF correction procedure was applied to all analyses (Ware, 1991). A beam spot size of 1 μm was used for all crystalline phases whereas both 1 μm and 10 μm beam spot sizes were used for glass analyses. The accumulation time was 100 s. As reported by Liu & O'Neill (2004), analytical accuracy and precision were checked by replicate measurements of three internationally recognized glass standards, GOR132G, T1G and KL2G (Jochum *et al.*, 2000).

Besides the oxides CaO, MgO, Cr_2O_3, Al_2O_3, SiO_2 and K_2O, FeO and Na_2O were included in the analytical procedure for all phases. FeO is a potential contaminant from the Fe_2O_3 sleeve if Fe were to diffuse right through the Pt capsule (see Liu & O'Neill, 2004); its absence was confirmed in all experiments. Na_2O is a good indicator of the quality of starting materials used. It concentrates in the melt with a content of 0·1–0·5 wt %, depending on the proportion of melt to solids in the experiment; such minor amounts are close to the limit of detection (~0·1 wt %), and as they also have almost negligible effect (Walter & Presnall, 1994; Liu *et al.*, in preparation) they have been ignored. To obtain the mean analyses of each phase together with standard deviations, which are presented in Table 3, individual analyses were first renormalized to 100%. This is appropriate for EDS analysis as most non-systematic contributions to analytical error are highly correlated between elements (e.g. variations in beam current, effects of sample coating, surface relief, etc.). Failure to renormalize before averaging would therefore result in a gross overestimation of analytical uncertainty.

Lithium and boron have potentially been cryptic contaminants of previous piston-cylinder studies, as these elements have not been amenable to microbeam analysis until recently. Li salts are sometimes used in noble-metal fabrication processes, and B could come from the Pyrex glass (it apparently diffuses readily through Pt). To check for any such contamination, Li and B were measured in the glasses in runs C-1472 and C-1516 (see Table 2 for experimental conditions) by laser ablation inductively coupled plasma mass spectrometry at RSES, ANU. The Li contents were 2·7 ± 0·3 ppm and 1·8 ± 0·1 ppm, respectively. The B contents were slightly higher at 65 ± 4 and 60 ± 1 ppm. These levels are very similar to those previously found in the experiments in the system CMAS ± K_2O (Liu & O'Neill, 2004), and should have a negligible effect on phase relations.

The Pt capsules from two runs, C-1469 and C-1476 (see Table 2 for experimental conditions) were checked for Fe, Cr and Ru (from RuO_2 used as an internal oxygen buffer in the former run) on a Cameca electron microprobe in wavelength-dispersive mode (WDS) at RSES, ANU; the results are shown in Fig. 1. Clearly, some Fe had diffused into the Pt capsules from the Fe_2O_3 sleeve, but only to approximately the middle of the capsule. The presence of reduced Fe in the Pt establishes that some reduction of the Fe_2O_3 sleeve has taken place, confirming that there really was a need for it. The diffusion profile shows that there is a limit to the run duration possible with our experimental assembly, as eventually Fe would diffuse right through the capsule into the charge (we checked for this possibility in every experiment by including Fe in the electron microprobe analytical routine). The presence of Ru is also confirmed by the electron microprobe analyses, indicating some reduction in the experiment. The quantity of metal Cr in the Pt capsules, however, is essentially negligible. This was not the case in some preliminary experiments carried out without the Fe_2O_3 sleeves, in which the presence of Cr in the Pt provided clear evidence for the reduction of Cr_2O_3.

Oxidation state of chromium

This study is specifically concerned with Cr as Cr^{3+}. As Cr^{2+} cannot be distinguished from Cr^{3+} by the analytical methods employed in this study (electron microprobe), its presence as a significant proportion of total Cr would fatally scramble the message from the experimental results. Thus a relatively high oxygen fugacity is a prerequisite to success in these experiments.

Initially we buffered oxygen fugacity internally by adding RuO_2 to the starting compositions (Table 1). During the course of the experiment, a small fraction of the RuO_2 was reduced to Ru metal. The oxygen fugacity of the Ru + RuO_2 buffer is close to Fe_3O_4–Fe_2O_3 at the temperatures of this study (O'Neill & Nell, 1997). Unfortunately, the presence of RuO_2 plus Ru in the experiment adds to the difficulty of finding melt pools with pristine glass (i.e. not modified by quench), and in subsequent experiments we relied only on the external Fe_2O_3 sleeve to prevent reduction. The amounts of Cr in all phases, including Ol and Melt, in these experiments are consistent with the amounts in the internally buffered experiments. Moreover, there is no apparent difference between the stoichiometries of crystalline phases in the Cr-bearing and Cr-free experiments, when these are calculated assuming all chromium in the former is Cr^{3+}.

Table 3: Experimentally observed phase compositions in wt %

Experiment	SiO_2	Al_2O_3	Cr_2O_3	MgO	CaO	K_2O
C-1550, 1360° C						
Ol(10)	42·70(0·10)	0·12(0·08)	0·15(0·07)	56·67(0·11)	0·35(0·03)	—
Sp(10)	0·46(0·08)	46·42(0·58)	26·85(0·74)	26·02(0·10)	0·26(0·05)	—
Opx(10)	55·26(0·15)	5·67(0·15)	1·49(0·13)	35·06(0·20)	2·52(0·13)	—
Melt(10)	51·82(0·11)	16·97(0·06)	0·22(0·07)	15·70(0·11)	13·68(0·07)	1·61(0·03)
C-1527, 1350° C						
Ol(10)	42·72(0·14)	0·24(0·08)	0·19(0·09)	56·47(0·09)	0·39(0·05)	—
Sp(14)	0·31(0·09)	52·90(0·40)	19·59(0·41)	26·98(0·10)	0·21(0·08)	—
Opx(22)	55·05(0·29)	6·44(0·29)	1·31(0·11)	34·65(0·30)	2·54(0·20)	—
Cpx(21)	52·27(0·23)	6·36(0·23)	1·51(0·12)	21·03(0·45)	18·83(0·52)	—
Melt(1)	51·61	18·32	0·16	14·67	14·37	0·85
D-82, 1340° C						
Ol(14)	42·91(0·21)	0·19(0·07)	0·10(0·08)	56·41(0·26)	0·39(0·09)	—
Sp(18)	0·37(0·15)	51·16(0·37)	21·47(0·40)	26·84(0·12)	0·16(0·06)	—
Opx(20)	55·21(0·21)	6·07(0·34)	1·31(0·11)	35·04(0·28)	2·38(0·15)	—
Cpx(17)	52·25(0·27)	6·39(0·37)	1·52(0·14)	20·90(0·38)	18·94(0·51)	—
Melt(13)	52·38(0·20)	19·90(0·35)	0·10(0·06)	11·58(0·31)	13·41(0·30)	2·62(0·13)
C-1511, 1330° C						
Ol(8)	42·99(0·19)	0·00(0·00)	0·12(0·05)	56·53(0·21)	0·36(0·03)	—
Sp(16)	0·33(0·10)	52·88(0·33)	20·20(0·36)	26·42(0·13)	0·16(0·06)	—
Opx(16)	55·13(0·29)	6·19(0·30)	1·33(0·12)	35·02(0·19)	2·34(0·10)	—
Cpx(16)	52·48(0·32)	6·07(0·42)	1·52(0·13)	21·10(0·38)	18·83(0·48)	—
Melt(12)	52·93(0·16)	22·00(0·40)	0·07(0·06)	9·22(0·36)	11·71(0·19)	4·08(0·16)
C-1499, 1360° C						
Ol(7)	42·74(0·14)	0·00(0·00)	0·14(0·09)	56·75(0·22)	0·37(0·04)	—
Sp(17)	0·52(0·11)	35·03(0·38)	39·34(0·39)	24·86(0·14)	0·25(0·06)	—
Opx(20)	55·86(0·36)	4·38(0·32)	1·79(0·17)	35·28(0·28)	2·70(0·36)	—
Cpx(17)	53·04(0·38)	4·83(0·27)	2·12(0·21)	22·28(0·31)	17·73(0·35)	—
Melt(13)	52·75(0·23)	15·40(0·14)	0·27(0·07)	15·98(0·17)	13·79(0·12)	1·80(0·05)
C-1481, 1350° C						
Ol(8)	42·68(0·17)	0·00(0·00)	0·22(0·08)	56·76(0·15)	0·33(0·03)	—
Sp(24)	0·34(0·09)	37·72(0·34)	36·91(0·33)	24·79(0·11)	0·25(0·06)	—
Opx(21)	55·50(0·34)	5·01(0·38)	1·84(0·18)	34·92(0·24)	2·74(0·25)	—
Cpx(21)	53·28(0·30)	5·21(0·33)	1·99(0·16)	23·43(0·34)	16·08(0·37)	—
Melt(20)	53·21(0·17)	17·04(0·11)	0·22(0·12)	13·85(0·18)	12·61(0·18)	3·06(0·08)
C-1478, 1340° C						
Ol(12)	42·89(0·10)	0·17(0·06)	0·12(0·10)	56·48(0·15)	0·34(0·06)	—
Sp(15)	0·45(0·20)	39·47(0·55)	34·38(0·52)	25·46(0·11)	0·24(0·08)	—
Opx(19)	55·66(0·33)	4·88(0·27)	1·71(0·20)	35·29(0·18)	2·45(0·11)	—
Cpx(21)	52·96(0·16)	5·10(0·15)	2·05(0·15)	22·03(0·47)	17·87(0·49)	—
Melt(21)	54·63(0·13)	18·81(0·16)	0·13(0·07)	10·57(0·13)	10·10(0·21)	5·76(0·16)
C-1480, 1320° C						
Ol(8)	42·81(0·13)	0·00(0·00)	0·06(0·04)	56·76(0·13)	0·37(0·05)	—
Sp(16)	0·62(0·27)	39·83(0·57)	34·21(0·49)	25·11(0·16)	0·23(0·07)	—

Experiment	SiO_2	Al_2O_3	Cr_2O_3	MgO	CaO	K_2O
Opx(17)	55·59(0·42)	4·77(0·38)	1·85(0·27)	35·30(0·36)	2·49(0·28)	—
Opx*(4)	55·59(0·50)	5·05(0·38)	1·51(0·42)	35·25(0·31)	2·61(0·26)	—
Cpx(16)	52·834(0·26)	5·19(0·20)	2·23(0·18)	21·74(0·24)	18·00(0·32)	—
Melt	—	—	—	—	—	—
C-1459, 1360° C						
Ol(6)	43·11(0·14)	0·00(0·00)	0·14(0·06)	56·43(0·12)	0·32(0·07)	—
Sp(8)	0·27(0·13)	24·73(0·48)	50·94(0·51)	23·82(0·14)	0·25(0·08)	—
Opx(15)	57·13(0·38)	2·83(0·25)	1·63(0·22)	35·72(0·41)	2·68(0·25)	—
Melt(8)	53·53(0·13)	13·38(0·06)	0·58(0·10)	16·99(0·11)	13·76(0·06)	1·77(0·09)
C-1414, 1360° C						
Ol(18)	42·70(0·14)	0·00(0·00)	0·37(0·11)	56·57(0·12)	0·35(0·02)	—
Sp(20)	0·33(0·08)	29·05(0·36)	45·87(0·46)	24·53(0·23)	0·23(0·05)	—
Opx(19)	56·56(0·21)	3·43(0·15)	1·52(0·12)	35·62(0·17)	2·86(0·18)	—
Cpx(20)	53·19(0·14)	4·67(0·28)	2·03(0·05)	22·56(0·26)	17·55(0·47)	—
Melt(15)	52·83(0·19)	14·40(0·14)	0·47(0·11)	16·83(0·16)	14·59(0·12)	0·87(0·06)
C-1472, 1350° C						
Ol(8)	42·80(0·14)	0·00(0·00)	0·17(0·05)	56·68(0·17)	0·35(0·06)	—
Sp(17)	0·35(0·09)	29·95(0·39)	45·06(0·30)	24·36(0·18)	0·27(0·05)	—
Opx(15)	56·44(0·22)	3·53(0·18)	1·78(0·21)	35·63(0·24)	2·62(0·10)	—
Cpx(17)	53·50(0·26)	4·12(0·24)	2·17(0·26)	22·95(0·24)	17·25(0·14)	—
Melt(9)	53·74(0·13)	15·39(0·09)	0·44(0·05)	14·75(0·04)	13·14(0·10)	2·54(0·08)
C-1449, 1340° C						
Ol(8)	42·64(0·23)	0·00(0·00)	0·12(0·06)	56·90(0·28)	0·34(0·05)	—
Sp(16)	0·39(0·11)	31·49(0·35)	43·24(0·45)	24·66(0·15)	0·22(0·06)	—
Opx(17)	56·49(0·20)	3·59(0·22)	1·73(0·16)	35·62(0·30)	2·57(0·13)	—
Cpx(22)	53·61(0·24)	4·05(0·22)	2·22(0·18)	22·47(0·34)	17·66(0·33)	—
Melt(13)	53·13(0·16)	16·30(0·18)	0·34(0·07)	13·42(0·28)	12·55(0·12)	3·26(0·06)
C-1469, 1330° C						
Ol(8)	42·94(0·12)	0·17(0·12)	0·01(0·02)	56·55(0·14)	0·34(0·07)	—
Sp(13)	0·37(0·15)	33·24(0·37)	41·38(0·44)	24·80(0·22)	0·21(0·09)	—
Opx(17)	56·56(0·29)	3·48(0·23)	1·77(0·17)	35·68(0·19)	2·52(0·18)	—
Cpx(23)	53·48(0·32)	4·33(0·36)	2·19(0·22)	22·41(0·34)	17·60(0·40)	—
Melt(6)	55·22(0·10)	18·45(0·16)	0·33(0·11)	10·01(0·17)	11·72(0·28)	4·26(0·11)
C-1489, 1360° C						
Ol(8)	42·83(0·11)	0·16(0·07)	0·40(0·05)	56·26(0·16)	0·35(0·03)	—
Sp(20)	0·44(0·09)	23·71(0·31)	51·97(0·42)	23·54(0·22)	0·34(0·05)	—
Opx(17)	56·92(0·23)	2·75(0·24)	1·74(0·14)	35·61(0·15)	2·99(0·07)	—
Cpx(19)	54·54(0·28)	3·34(0·20)	2·09(0·16)	25·53(0·53)	14·49(0·53)	—
Melt(15)	53·20(0·13)	13·21(0·12)	0·44(0·07)	17·61(0·26)	14·36(0·26)	1·19(0·05)
C-1463, 1350° C						
Ol(6)	42·79(0·12)	0·00(0·00)	0·25(0·17)	56·61(0·14)	0·35(0·04)	—
Sp(14)	0·46(0·15)	21·96(0·41)	53·87(0·40)	23·35(0·20)	0·37(0·06)	—
Opx(19)	57·10(0·38)	2·29(0·23)	1·82(0·30)	35·95(0·24)	2·85(0·14)	—
Cpx(25)	54·57(0·35)	2·75(0·29)	2·20(0·32)	23·92(0·33)	16·56(0·39)	—
Melt(20)	54·92(0·15)	13·79(0·13)	0·30(0·07)	15·16(0·12)	12·85(0·10)	2·97(0·09)

Table 3: continued

Experiment	SiO_2	Al_2O_3	Cr_2O_3	MgO	CaO	K_2O
C-1476, 1330°C						
Ol(7)	42·92(0·20)	0·00(0·00)	0·17(0·06)	56·55(0·15)	0·36(0·03)	—
Sp(13)	0·51(0·18)	27·29(0·50)	47·93(0·55)	23·93(0·15)	0·34(0·10)	—
Opx(16)	57·16(0·35)	2·68(0·33)	1·52(0·19)	35·80(0·28)	2·84(0·28)	—
Opx*(3)	57·19(0·30)	2·81(0·37)	1·49(0·20)	35·52(0·32)	2·99(0·24)	—
Cpx(22)	54·05(0·47)	3·38(0·51)	2·09(0·22)	23·29(0·39)	17·19(0·47)	—
Melt(11)	55·20(0·20)	16·06(0·20)	0·18(0·07)	12·53(0·15)	10·92(0·17)	5·11(0·09)
C-1516, 1380°C						
Ol(12)	42·83(0·12)	0·16(0·05)	0·40(0·08)	56·23(0·16)	0·39(0·04)	—
Sp(18)	0·44(0·12)	13·74(0·22)	63·14(0·29)	22·31(0·15)	0·37(0·07)	—
Opx(16)	57·94(0·28)	1·56(0·25)	1·27(0·19)	36·10(0·22)	3·12(0·10)	—
Cpx(16)	56·62(0·16)	1·73(0·10)	1·61(0·10)	30·73(0·39)	9·31(0·32)	—
Melt(15)	54·80(0·18)	10·23(0·17)	0·59(0·09)	18·15(0·25)	14·15(0·16)	2·08(0·04)
C-1512, 1370°C						
Ol(8)	42·77(0·11)	0·00(0·00)	0·34(0·10)	56·50(0·18)	0·39(0·06)	—
Sp(20)	0·44(0·12)	16·58(0·24)	60·38(0·26)	22·25(0·14)	0·35(0·08)	—
Opx(19)	57·75(0·24)	1·77(0·19)	1·37(0·15)	36·11(0·16)	3·00(0·07)	—
Cpx(14)	55·74(0·24)	2·15(0·24)	1·80(0·17)	27·68(0·38)	12·63(0·38)	—
Melt(14)	54·99(0·10)	11·74(0·17)	0·41(0·11)	16·49(0·12)	13·34(0·21)	3·02(0·05)
C-1515, 1360°C						
Ol(8)	41·69(0·16)	0·00(0·00)	0·44(0·06)	57·52(0·16)	0·35(0·06)	—
Sp(17)	0·71(0·19)	19·79(0·59)	55·32(0·59)	23·82(0·17)	0·37(0·07)	—
Opx(16)	56·96(0·32)	1·30(0·30)	1·45(0·23)	37·43(0·34)	2·86(0·35)	—
Cpx(12)	54·88(0·32)	2·31(0·36)	1·98(0·31)	26·48(0·27)	14·36(0·40)	—
Melt(15)	55·33(0·14)	12·93(0·12)	0·32(0·08)	15·18(0·10)	12·23(0·11)	4·01(0·06)

Ol(12) is phase name followed by the number of individual EDS analyses, which were normalized to 100% to calculate the mean and standard deviations; these are given as 42·72(0·12), for example, which should be read as 42·72 ± 0·12. Melt was present but could not be analysed in C-1480, and only one melt pool was large enough to produce an analysis in C-1527. In experiments with zoned Cpx and Sp, reported analyses are from the 'sandwiching' layers. In two experiments, Opx analyses from 'sandwiched' layers, indicated by an asterisk, are also given.

Attainment of equilibrium

Our previously reported results in the Cr-free system (CMAS ± K_2O; Liu & O'Neill, 2004) show that the experimental technique used in this study (i.e. the sandwich method with pre-crystallized solid phases) is capable of attaining well-equilibrated phase assemblages; exceptions were for melt compositions with relatively high SiO_2 that were not in equilibrium with Ol, and experiments with very low melt fractions. The evidence for disequilibrium is obvious, as a reaction layer with pyroxenes that change composition across the layer is formed [see discussion by Liu & O'Neill (2004)]. For most of the experiments of that study, the only sign of disequilibrium was some minor zoning of Al_2O_3 in the cores of larger pyroxene crystals grown in the melt layer of the sandwich.

However, Cr-containing systems are notoriously difficult to equilibrate (O'Neill, 1981; Nickel, 1986; Klemme & O'Neill, 2000; Girnis *et al.*, 2003), and a more troublesome equilibration problem occurs in a few of the present experiments where the extent of partial melting is low, resulting in a large degree of crystallization, mainly of Cpx + Sp, from the glass in the sandwiched layer. These Cpx and Sp generally have low and variable Cr/(Cr + Al), being lowest in the cores of larger crystals. This is expected, as the glass starting compositions have low Cr_2O_3, hence the first crystals forming from such compositions have low Cr_2O_3. Having once crystallized, inter-diffusion of Cr and Al is then apparently too sluggish to permit complete re-equilibration. However, the compositions of both the smaller crystals and the rims of the larger crystals approach the compositions of the

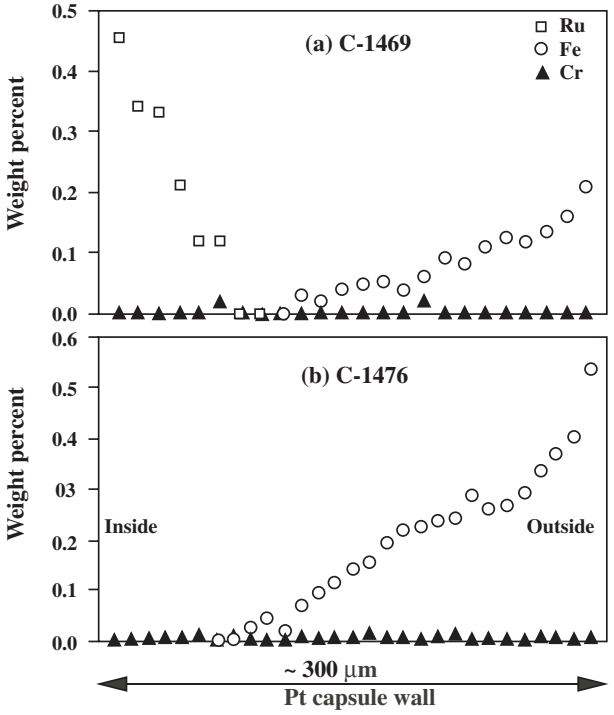

Fig. 1. Electron microprobe analyses across the walls of two Pt capsules (WDS method): (a) C-1469 with internal oxygen fugacity buffer of RuO_2; (b) C-1476 without internal oxygen fugacity buffer. (See Table 2 for experimental details.)

phases in the crystalline layers of the sandwich, which are generally very homogeneous (Table 3). Examples of this behaviour are shown in Fig. 2 for Cpx in experiments C-1476 and C-1480 and for Sp in C-1463. Interestingly, the Mg/(Ca + Mg) ratio of the Cpx closely follows the Cr/(Cr + Al) ratio. The significance of this will be discussed below. Because of the bulk composition, only a few small grains of Opx crystallized in the 'sandwiched' glass layers of these experiments, but these crystals are indistinguishable in composition from those in the crystalline sandwiching layers, as shown for runs C-1480 and C-1476 in Table 3.

We therefore make the assumption in interpreting these experiments that the outermost rims of the crystals in the sandwiched layer that are zoned in Cr/(Cr + Al) would be similar to the homogeneous crystals in the crystalline layers, and it is these compositions that are in equilibrium with the melt. This interpretation is consistent with the evidence from the Opx compositions.

Those experiments with a high degree of melting (which are also generally at higher temperatures) do not have this problem and the equilibrium compositions of the solid phases are easily obtained. This is important, as the good internal consistency between these experiments and those with zoned crystals at low partial melting extents is another indicator that our assumption regarding the latter is appropriate.

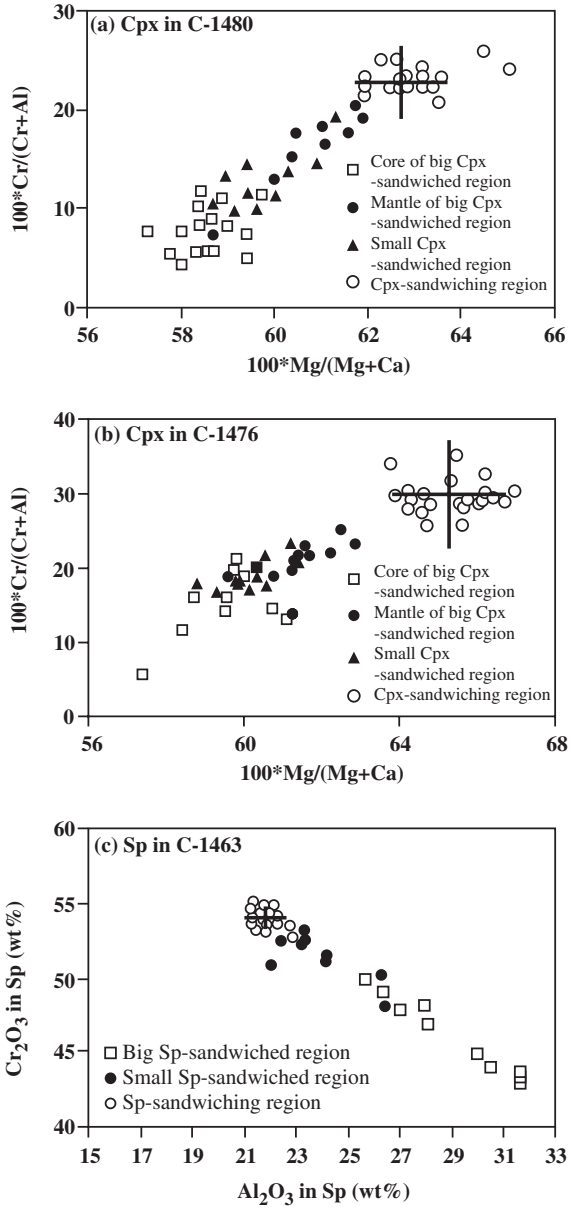

Fig. 2. Covariation of Mg/(Mg + Ca) with Cr/(Cr + Al) in clinopyroxene (a, b), and of Al_2O_3 and Cr_2O_3 in Sp (c) in incompletely equilibrated experiments, which are all at relatively low temperatures and contain only low melt fractions (e.g. the amount of melt in C-1480 was too small for its composition to be determined). It should be noted that these are the worst-case examples, and that the compositions of minerals in most experiments are homogeneous. The average inferred equilibrium compositions, plotted as error bars (± 2 SD) from the data in Table 3, are obtained from the 'sandwiching regions' of the experiments. These compositions fall at the ends of the compositional trends obtained from crystals that crystallize from glass in the 'sandwiched regions', which are compositionally variable as indicated.

EXPERIMENTAL RESULTS

Table 2 summarizes the starting materials, the experimental techniques, the run conditions and the results of the experiments; the K_2O content of the melts and the

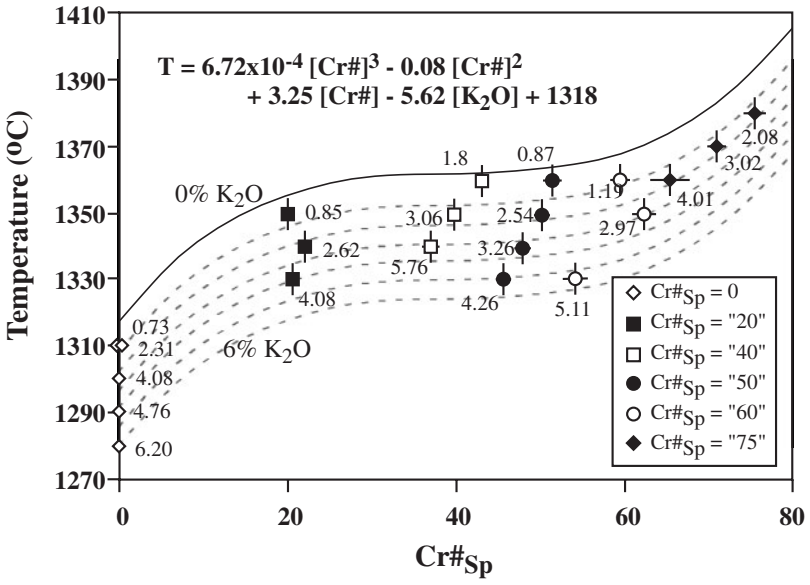

Fig. 3. The effect of $Cr\#_{sp}$ on the solidus temperature. Numbers adjacent to each symbol are wt % K_2O in the melt. Contours of K_2O at 1 wt % intervals are from regression of the data [equation (9)].

calculated temperature using different geothermometers from the literature are also shown in Table 2. Out of 19 experiments, 17 display melt coexisting with the full Sp-lherzolite phase assemblage, whereas the remaining two experiments have melt coexisting with Ol + Opx + Sp. The amount of melt in one experiment with the full Sp-lherzolite phase assemblage (C-1480) was too low to be properly analysed. The phase composition data are compiled in Table 3.

Melt composition

The phase assemblage Ol + Sp + Opx + Cpx + Melt has two degrees of freedom in the system CMAS–Cr_2O_3–K_2O at a specified pressure, which we have chosen to describe using the two variables of K_2O in the melt (here labelled as $[K_2O]$) and $Cr\#_{sp}$; consequently, the solidus temperature and the composition of the melt can all be described using these two variables. By fitting the data to empirical equations in $[K_2O]$ and $Cr\#_{sp}$, we can then extrapolate the data to zero $[K_2O]$ to find the main object of this study, the composition of melt along the spinel-lherzolite solidus as a function of $Cr\#_{sp}$. The degree of extrapolation is modest, such that any inadequacies in our empirical polynomial equations from the point of view of thermodynamic theory have no significant effects on the results.

The solidus temperature is given by

$$T_{\text{solidus}}\,(^{\circ}\text{C}) = 1318 - 5{\cdot}62[\text{K}_2\text{O}] + 3{\cdot}25\text{Cr}\#_{\text{sp}} - 0{\cdot}08(\text{Cr}\#_{\text{sp}})^2 + 6{\cdot}72\times10^{-4}(\text{Cr}\#_{\text{sp}})^3. \quad (9)$$

This was obtained from a multiple non-linear least-squares fit to the data in both the system CMAS–K_2O (five data points, from Liu & O'Neill, 2004) with $[K_2O]$ <7 wt %, and the system CMAS–Cr_2O_3–K_2O (16 data points, from Table 3). The data were weighted assuming uncertainties of ±5°C in experimental temperature, and as reported in $[K_2O]$ and $Cr\#_{sp}$. The reduced chi-squared value (χ^2_ν) for the regression with these weights was 1·2, demonstrating a good fit, as shown in Fig. 3. The addition of Cr_2O_3 raises the solidus temperature, as expected for a refractory (or highly compatible) component that stabilizes the solid phases relative to melt. The increase is not linear, being strong at low $Cr\#_{sp}$, weak at intermediate $Cr\#_{sp}$ and strong again at high $Cr\#_{sp}$, hence the need for a three-term polynomial in $Cr\#_{sp}$.

For describing the melt compositions at the solidus, it is apparent from the raw data that the effect of K_2O in the system CMAS–Cr_2O_3–K_2O is rather different from that in the system CMAS–K_2O (Fig. 4). This may be due to interactions between K_2O and Al_2O_3 in the melt. In any case, to obtain a reasonable empirical fit to the data, we fitted the Cr-containing and Cr-free experiments separately. We also found from a preliminary fitting that one experiment, C-1469, has a somewhat anomalous melt composition, being too high in Al_2O_3 and SiO_2 and low in MgO compared with predictions from the fit obtained from the other 15 data points (Fig. 5). This experiment is at the low-temperature end of its particular $Cr\#_{sp}$ series (Experiment Set 1 in Table 2), and contained a relatively small amount of melt, such that it is possible that the melt composition may have been modified by some quench crystallization. So as not to bias the empirical

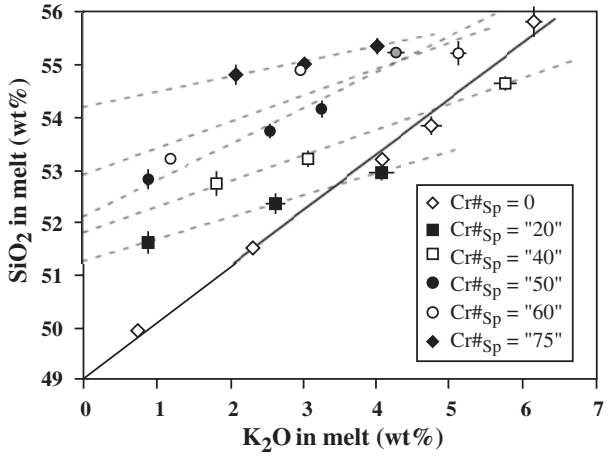

Fig. 4. Correlation of K_2O with SiO_2 in melts in the system CMAS–K_2O (bold continuous line) and in the system CMAS–Cr_2O_3–K_2O. The data for each 'set' of experiments (identified by the average $Cr\#_{sp}$ in the run products) are linked by the fine dashed lines; these lines are to guide the eye only, as the actual $Cr\#_{sp}$ varies within each set. The anomalous Run C-1469 is shown in grey.

extrapolation of the other data, it was removed from the regression. For the remaining 15 data points in the system CMAS–Cr_2O_3–K_2O we obtained (for $Cr\#_{sp} \geq 20$)

$$[SiO_2] = 49{\cdot}8 + 0{\cdot}53[K_2O] + 0{\cdot}051Cr\#_{sp} \; (\chi^2_\nu = 1{\cdot}2) \quad (10)$$

$$[Al_2O_3] = 25{\cdot}9 + 0{\cdot}62[K_2O] - 0{\cdot}535Cr\#_{sp} + 9{\cdot}41 \times 10^{-3}(Cr\#_{sp})^2 - 7{\cdot}09 \times 10^{-5}(Cr\#_{sp})^3 \; (\chi^2_\nu = 2{\cdot}7) \quad (11)$$

$$[MgO] = 6{\cdot}8 - 1{\cdot}84[K_2O] + 0{\cdot}685Cr\#_{sp} - 1{\cdot}42 \times 10^{-2}(Cr\#_{sp})^2 + 9{\cdot}84 \times 10^{-5}(Cr\#_{sp})^3 + 1{\cdot}39 \times 10^{-2}[K_2O]Cr\#_{sp} \; (\chi^2_\nu = 2{\cdot}7) \quad (12)$$

$$[CaO] = 14{\cdot}8 - 0{\cdot}86[K_2O] + 0{\cdot}012Cr\#_{sp} (\chi^2_\nu = 1{\cdot}0). \quad (13)$$

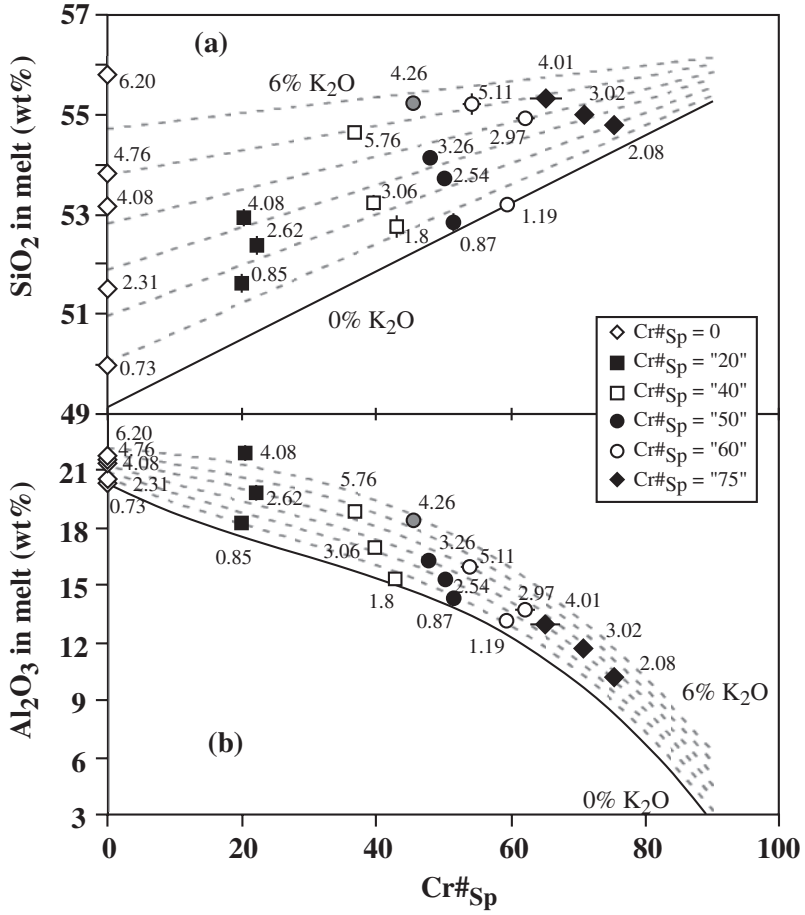

Fig. 5. The effect of $Cr\#_{sp}$ on melt composition: (a) SiO_2; (b) Al_2O_3; (c) MgO; (d) CaO. One anomalous run (C-1469 with a K_2O content of 4·26%) is shown in grey. Smoothed contours of K_2O in the melt are drawn from 0 to 6 wt %, using equations (10)–(13) in the text and information from the system CMAS + K_2O from Liu & O'Neill (2004).

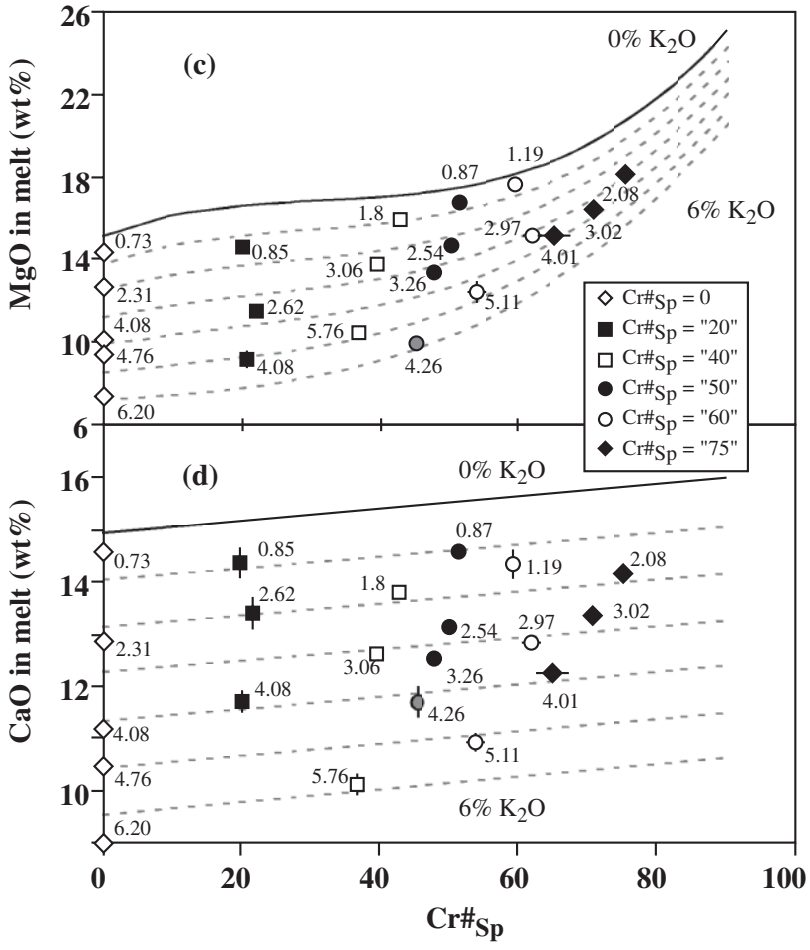

Fig. 5. Continued

These empirical equations then allow the melt composition in the system CMAS–Cr_2O_3 to be calculated as a function of $Cr\#_{sp}$. The average difference between the calculated melt composition using these equations and the experimentally observed melt composition is 0·23 wt % for SiO_2, 0·31 wt % for Al_2O_3, 0·32 wt % for MgO and 0·13 wt % for CaO. The regressed melt compositions are shown in Fig. 5a–d.

Melt compositions in the system CMAS–Cr_2O_3 derived from the experiments in the system CMAS–Cr_2O_3–K_2O by equations (10)–(13) are projected from Ol onto the plane Di–JdCaTsLc–Qz (Fig. 6a), from Di onto the plane Ol–JdCaTsLc–Qz (Fig. 6b) and from An onto the plane Di–Ol–Qz (Fig. 6c). To handle Cr in these plots, the Cr_2O_3 contents of the melts were subtracted and other oxides were renormalized to 100 wt %. (An alternative procedure would be to subtract a $Mg_2Cr_2O_4$ component as this would be an early crystallizing phase. Doing this would make the melts very slightly more Qz-normative, relatively, from 0·17 mol % more Qz-normative at $Cr\#_{sp} = 20$, to 0·96 mol % more Qz-normative at $Cr\#_{sp} = 80$.)

The most striking features of the melt compositions in the system CMAS–Cr_2O_3 are the increasing Di component (Fig. 6a and c), the increasing Hy component and the generally quartz-normative nature (Fig. 6b) at 1·1 GPa.

The isobarically invariant melt produced by the Sp-lherzolite assemblage in the system CMAS at 1·1 GPa is an olivine-normative tholeiite (Presnall *et al.*, 1979; Walter & Presnall, 1994; Liu & O'Neill, 2004). However, the melt composition reaches the join An–Hy and becomes Qz-normative at $Cr\#_{sp} = 20$. As Cr_2O_3 is added to the system, the Al_2O_3 content of the melt drops sharply, so that the An component of the melt decreases. The effect of less An component, coupled with the almost negligible effect of Cr_2O_3 on the CaO content of the melt [equation (13)], means that more CaO is available to form Di. An increase in Di component in turn requires more MgO, but this is more than compensated for by the effect that Cr_2O_3 has on

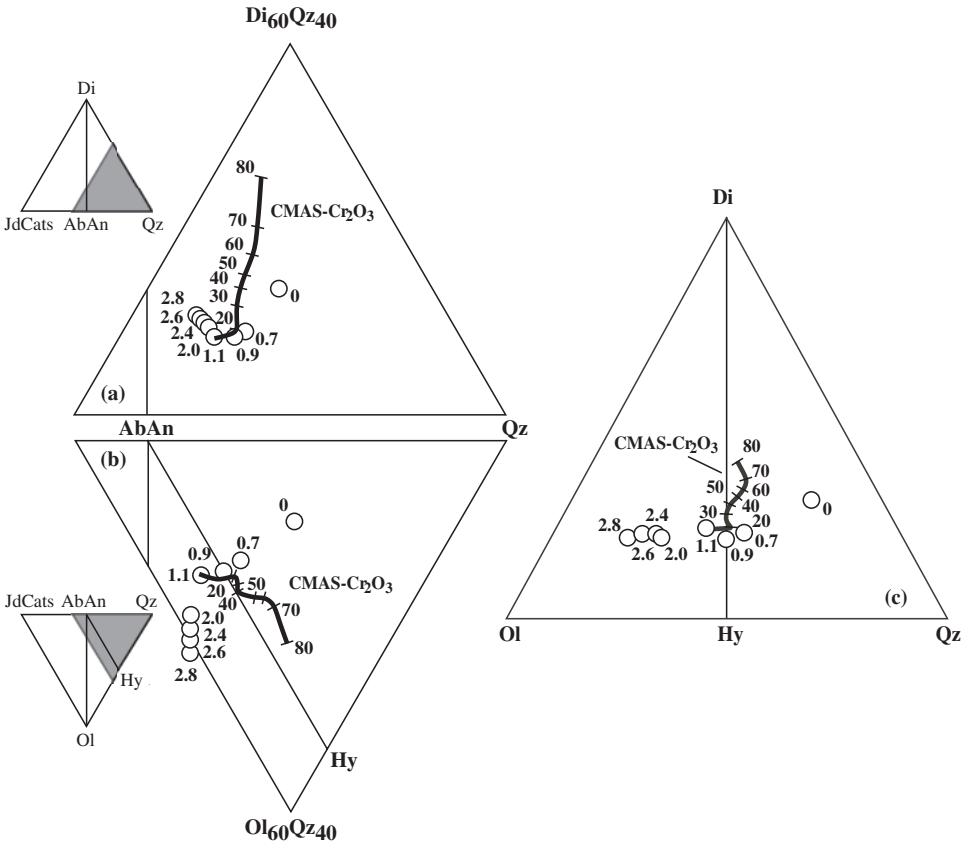

Fig. 6. The multiply saturated (Ol + Opx + Cpx + Sp) melt composition in the system CMAS–Cr_2O_3: (a) projected from Ol onto the plane Di–JdCats–Qz; (b) projected from Di onto the plane JdCats–Qz–Ol; (c) projected from AbAn onto the plane Ol–Di–Qz. The projection procedure of Falloon & Green (1988) is used, with Cr_2O_3 handled by subtracting it from the melt composition and renormalizing to 100%. The melt composition at $Cr\#_{sp} = 0$ is from Liu & O'Neill (2004), other compositions are calculated using equations (10)–(13). Numbers along the curve are $Cr\#_{sp}$. Also shown as open circles are the compositions of melt in equilibrium with Ol + Opx + Cpx + Sp (or An in place of Sp at $P \leq 0{\cdot}9$ GPa) in the system CMAS as a function of pressure (in GPa). Data at 0 GPa from Longhi (1987); at 2·4, 2·6 and 2·8 GPa from Gudfinnsson & Presnall (1996); and at other pressures from Walter & Presnall (1994).

increasing MgO (equation (12)]. The net result is an increase in the Hy + Ol or Hy + Qz components of the melt. An interesting point is that for $Cr\#_{sp} \geq 20$, the extra MgO and SiO_2 are approximately in the proportion of 1:1, so that in the projection from Di (Fig. 6b) the melt composition changes along a line almost parallel to the An–Hy join.

Also shown in Fig. 6 is the change with pressure of the composition of the melt along the five-phase univariant curve in the system CMAS, where melt is in equilibrium with Ol + Opx + Cpx + Sp (or with Ol + Opx + Cpx + An at $P \leq 0{\cdot}9$ GPa). Whereas the effect of pressure on melt compositions in the range 0–2·8 GPa is of similar magnitude to the effect of changing $Cr\#_{sp}$, the compositional changes are very distinct. As emphasized by the projection in Fig. 6c, increasing pressure causes multiply saturated melt compositions to become richer in normative Ol, whereas the dominant effect of increasing $Cr\#_{sp}$ is to make the melt richer in normative Di.

Ol and Sp compositions

The amount of Cr as Cr_2O_3 in Ol increases with $Cr\#_{sp}$, reaching 0·4 wt % at $Cr\#_{sp} = 60$; the amount of CaO, however, is constant (0·35 ± 0·05). In our preliminary unbuffered experiments without Fe_2O_3 sleeves (not reported), Ol had higher Cr contents (up to ∼0·8 wt % Cr_2O_3 at $Cr\#_{sp} = 60$), indicative of Cr^{2+}.

The spinel in the system CMAS–Cr_2O_3 (± K_2O) is a simple binary solid solution between $MgAl_2O_4$ and $MgCr_2O_4$. The electron microprobe analyses return small and variable amounts of SiO_2 and CaO, which are probably spurious, caused by the generally small size of spinel crystals (typically 3–15 μm in diameter).

Pyroxene compositions

Al_2O_3 and Cr_2O_3

The relationship of Cr and Al in pyroxenes observed in this study is shown in Fig. 7. For comparison, the data in

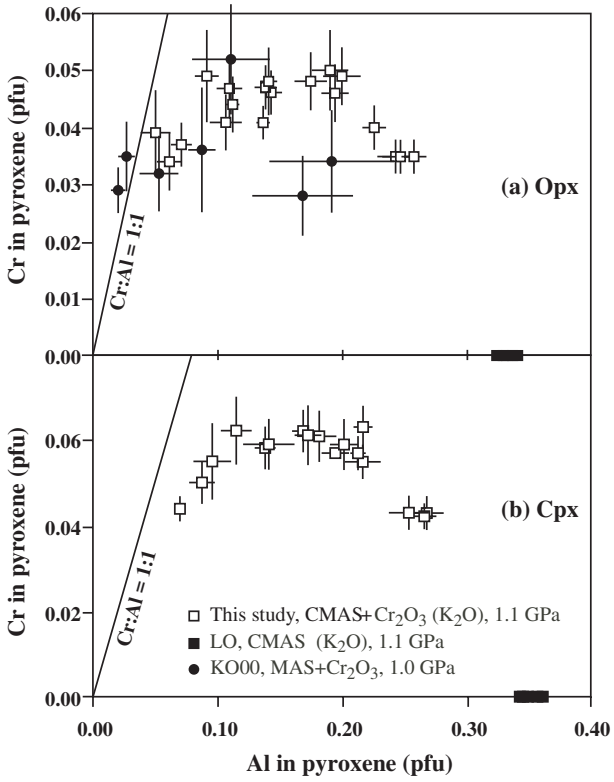

Fig. 7. Covariation of Cr and Al in orthopyroxenes (a) and clinopyroxenes (b). Data sources: KO00, Klemme & O'Neill (2000); LO, Liu & O'Neill (2004). pfu, per formula unit of six oxygens. All chromium has been assumed to be Cr^{3+}.

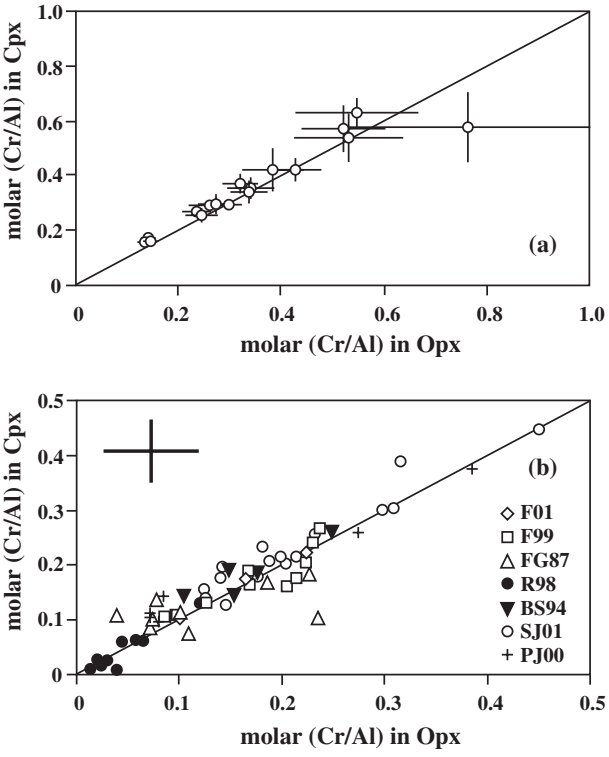

Fig. 8. The partitioning of Cr/Al between Opx and Cpx at near-solidus conditions, 1·0–1·5 GPa: (a) this study; (b) compositionally complex systems. The average 1 SD uncertainty observed in our study is plotted in (b) to facilitate the data comparison. Data sources: F01, Falloon *et al.* (2001); F99, Falloon *et al.* (1999); FG87, Falloon & Green (1987) [the revised data of Falloon *et al.* (2001) are used here]; R98, Robinson *et al.* (1998); BS94, Baker & Stolper (1994); SJ01, Schwab & Johnston (2001); PJ00, Pickering-Witter & Johnston (2000). The pressure in all studies except that by Robinson *et al.* (1998; 1·5 GPa) and this study (1·1 GPa) is 1·0 GPa. Only multiply saturated experiments are shown.

the system MAS–Cr_2O_3 at subsolidus conditions from Klemme & O'Neill (2000) are also shown.

The relationship between Cr and Al in Opx is complex (Fig. 7a). When Cr is added to the systems MAS and CMAS, the Cr content in Opx first increases, causing the expected negative correlation with Al, but then reaches a maximum value, and at very high Cr/Al ratios both Cr and Al decrease, causing a positive correlation between them. This curious behaviour was previously observed by Nagata *et al.* (1983) and Witt-Eickschen & Seck (1991) in natural peridotites, and its thermodynamic explanation has been given quantitatively by Klemme & O'Neill (2000).

The relationship between Al and Cr in Cpx, shown in Fig. 7b, is similar to that observed in Opx. It follows that the partitioning of Al^{3+} and Cr^{3+} between Opx and Cpx should also be similar. This is demonstrated in Fig. 8a, where all experimental data in the simple systems plot close to the 1:1 line. Most experimental data from the literature at near-solidus temperatures (which are all in complex multicomponent systems) also plot close to the 1:1 line (Fig. 8b), but the experiments of Falloon & Green (1987) at 1·0 GPa define an almost horizontal trend, implying that the Cr/Al ratio in Cpx does not change with that ratio in Opx. Possibly this is due to the short experimental run durations (<24 h in most cases), which may be long enough to effect compositional change in the Opx, but not in the Cpx. This would be consistent with the observation in this study that the Cpx in the sandwiched layer in several of the experiments at low degrees of melting is zoned in Cr/Al, whereas Opx is homogeneous.

CaO and MgO

The exchange of Ca and Mg between Opx and Cpx is the basis of the two-pyroxene geothermometer, the main means of estimating temperatures of equilibration in lherzolitic assemblages. Previous experimental studies have mostly been at relatively low temperatures (Gasparik, 1984; Nickel *et al.*, 1985; Sen, 1985; Brey *et al.*, 1990) or in very simple chemical systems (Lindsley & Dixon, 1976; Mori & Green, 1976; Nickel & Brey,

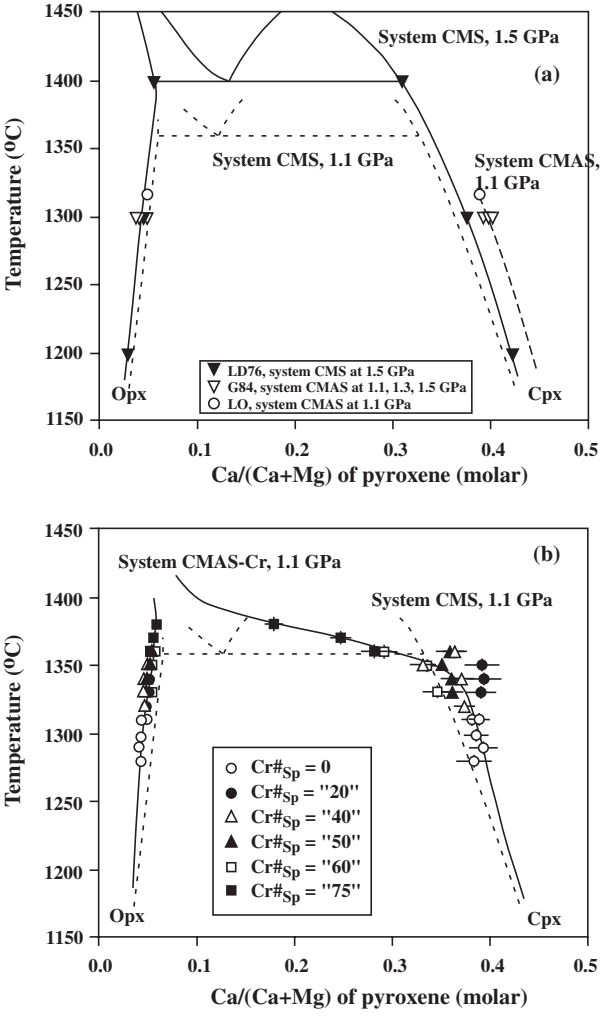

Fig. 9. Ca–Mg partitioning between Opx and Cpx: (a) phase relations in the systems CMS and CMAS; (b) inferred phase relations in the system CMAS–Cr_2O_3. For clarity, the curve for the CaO content in Opx in the system CMAS at 1·1 GPa is omitted in (a). Data sources: LD76, Lindsley & Dixon (1976); G84, Gasparik (1984). Cpx in the highest temperature, highest $Cr\#_{sp}$ runs becomes distinctly subcalcic.

1984). The experimental observations here offer an opportunity to evaluate the two-pyroxene equilibrium at relatively high temperatures and in a chemical system of intermediate complexity.

Pyroxene phase relationships in the system CMS and CMAS at 1·1–1·5 GPa are shown in Fig. 9a. Data in the system CMAS are from assemblages saturated in Sp, and therefore these pyroxenes have the maximum amount of dissolved alumina for Ol-containing assemblages. The Ca/(Ca + Mg) ratio of Opx is almost independent of pressure and alumina content, but strongly dependent on temperature. The Ca/(Ca + Mg) ratio of Cpx is also almost independent of pressure, as illustrated by the data of Gasparik (1984); it, however, depends on both temperature and alumina. The presence of Al_2O_3 increases Ca/(Ca + Mg) in Cpx.

The geometry of the phase relations between Opx and Cpx is strongly influenced by the solvus that exists (mostly metastably) between low-Ca Cpx and high-Ca Cpx. The solidus of the Ol + Opx + Cpx + Sp assemblage in the system CMAS at 1·1 GPa is ~1320°C (Liu & O'Neill, 2004), which is much lower than the crest of the solvus in CMS (~1450°C, from Nickel & Brey, 1984, fig. 5), and also lower than the temperature at which low-Ca Cpx becomes stable (~1360°C). Thus in CMAS saturated with Ol + Sp only Opx and high-Ca Cpx exist stably. There are no experimental data in the literature that can be used to define the phase relationships at 1·1 GPa at temperatures >1320°C, except those in the pure CMS system. However, adding Cr_2O_3 to CMAS raises the solidus, permitting access to this temperature region, albeit at lower Al_2O_3 contents.

Our experimental data are plotted in Fig. 9b. It appears that the addition of Al_2O_3 and Cr_2O_3 to the system CMS must lower the crest of the Cpx solvus, such that the Cpx compositions in the highest temperature experiments are decidedly subcalcic. The phase relationship is hence drawn as shown in Fig. 9b. This geometry is similar to the phase relationship observed at higher pressures (> ~1·8 GPa) in the system CMS (Mori & Green, 1976; Nickel & Brey, 1984; Longhi & Bertka, 1996). Partial melting studies using natural lherzolite compositions (Takahashi & Kushiro, 1983; Falloon & Green, 1988, and unpublished data) suggested that the Cpx solvus becomes metastable relative to Cpx + Opx at a pressure between 1·5 and 1·8 GPa.

Experiments with variable Cpx compositions display remarkably tight correlations between Ca/(Ca + Mg) and Cr/(Cr + Al) (Fig. 2). The increase of Ca with Al in Cpx is similar to the difference observed in Cpx compositions in equilibrium with Opx between the systems CMS and CMAS, as shown in Fig. 9a. We therefore interpret these correlations to be due to initial differences in Cr/(Cr + Al) in Cpx being preserved as a result of sluggish diffusion rates for Cr and Al, with Ca and Mg adjusting to the local Cr/(Cr + Al) ratio to maintain metastable local equilibrium with Opx.

The experimental data on pyroxene compositions can be used to calculate temperatures from two-pyroxene geothermometers (Table 2). The difference between measured and calculated temperatures increases as a function of $Cr\#_{sp}$ (Fig. 10). This is not unexpected, as these geothermometers do not explicitly account for the effect of Al_2O_3 in pyroxenes. As discussed above, the decreasing Al_2O_3 in Cpx (which correlates with $Cr\#_{sp}$) narrows the two-pyroxene miscibility gap (Fig. 9), such that formulations not accounting for this effect will show systematically rising calculated temperature with decreasing Al_2O_3 in Cpx. The composition of Opx is less

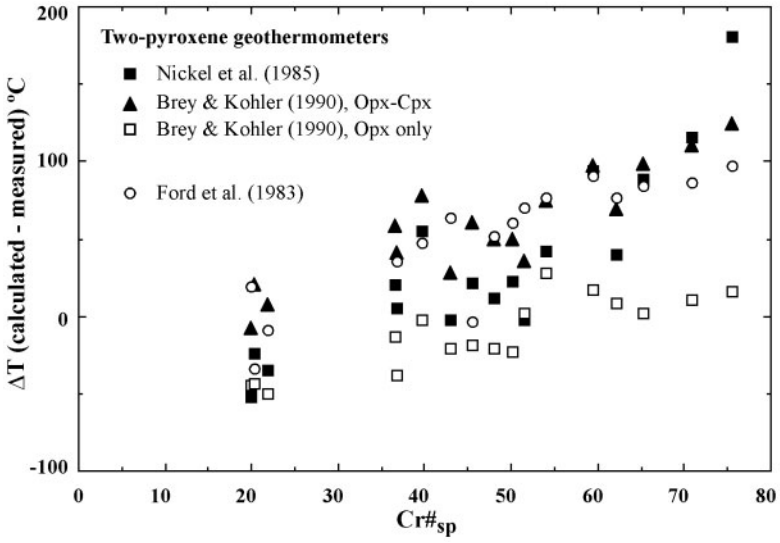

Fig. 10. Testing various two-pyroxene geothermometers and the MgO 'magmathermometer' of Ford *et al.* (1983): the difference between calculated and experimentally measured temperatures, plotted against $Cr\#_{sp}$.

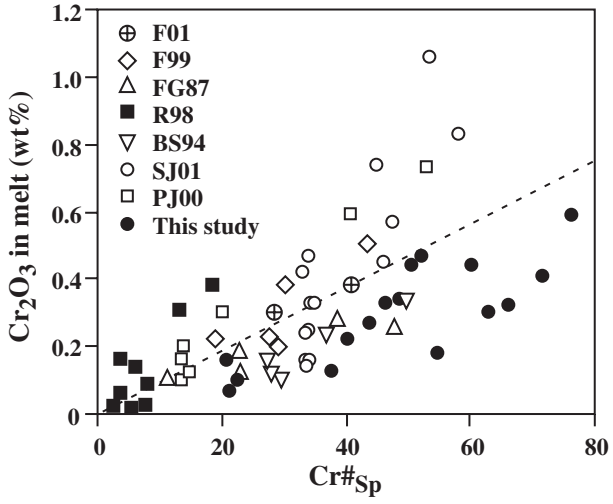

Fig. 11. Observed Cr (as Cr_2O_3) in melts from experiments in the system CMAS–Cr_2O_3–K_2O as a function of $Cr\#_{sp}$ compared with experiments on natural compositions. Data sources: F01, Falloon *et al.* (2001); F99, Falloon *et al.* (1999); FG87, Falloon & Green (1987) [we use the revised data of Falloon *et al.* (2001)]; R98, Robinson *et al.* (1998); BS94, Baker & Stolper (1994); SJ01, Schwab & Johnston (2001); PJ00, Pickering-Witter & Johnston (2000). The pressure in all studies except that by Robinson *et al.* (1998; 1·5 GPa) and this study (1·1 GPa) is 1·0 GPa. Only multiply saturated experiments are shown.

sensitive to Al_2O_3; hence the 'Opx-only' geothermometer of Brey & Kohler (1990) shows a relatively small variation with $Cr\#_{sp}$. Coincidentally, the 'magmathermometer' of Ford *et al.* (1983) shows an almost identical trend with $Cr\#_{sp}$, suggesting that this empirical method of estimating temperatures will be subject to a systematic error that depends on $Cr\#_{sp}$ in natural compositions too.

Cr in the melt

The amount of Cr in the melt (as Cr_2O_3) is given by the regression as

$$['Cr_2O_3'] = 9{\cdot}0 \times 10^{-3} Cr\#_{sp} - 9{\cdot}6 \times 10^{-4} [K_2O] Cr\#_{sp}. \quad (14)$$

The value of χ^2_ν for the regression is 0·74 (16 data points), indicating that our data fit this simple equation very well within their analytical uncertainty (Table 3). Our data include experiments both buffered by Ru + RuO_2 and unbuffered. That both types of experiments can be fitted by the same equation implies that the Cr in the unbuffered experiments is in a similar oxidation state to that in the buffered experiments, i.e. mostly as Cr^{3+}. As might be expected, the primary control on Cr^{3+} in the melt is $Cr\#_{sp}$, although the effect of $[K_2O]$, described by the second term in equation (14), is statistically significant. At more reducing conditions, the amount of Cr^{2+} in the melt would not be negligible, and total analysed 'Cr_2O_3' should lie above the curve established by our experiments.

The experimentally observed 'Cr_2O_3' contents in the melts in the current study are plotted in Fig. 11 vs $Cr\#_{sp}$, along with data from several partial melting studies on natural compositions in the literature. All these literature studies used an inner graphite capsule inside a sealed Pt capsule. This arrangement does not buffer oxygen fugacity, as this is given by $C_{(graphite)} + O_2 = CO_2$ and P_{CO_2} is generally not known. The maximum f_{O_2} occurs when $P_{CO_2} = P_{total}$. Thus f_{O_2} in such experiments could be

relatively oxidizing when P_{CO_2} is near saturation, but proportionally lower if P_{CO_2} is low. Because f_{O_2} in experiments on natural systems affects the behaviour of Fe, and near-saturation levels of CO_2 also have an effect on phase relations (small but not entirely negligible at ~1 GPa; see Liu, 2003), it is instructive to use the partitioning of Cr between spinel and melt [buffered by olivine + orthopyroxene; see equation (4)] to infer something about f_{O_2} and P_{CO_2} in these experiments. Differences in f_{O_2}/P_{CO_2} might account for some of the differences in results; in particular, higher Cr in the melt suggests Cr^{2+}, hence low f_{O_2} and P_{CO_2}. Figure 11 shows that Cr partitioning is variable in many studies, suggesting a lack of consistency in f_{O_2}/P_{CO_2} even within one study.

Cr^{3+} partitioning

The partition coefficients of total Cr (i.e. as both Cr^{3+} and Cr^{2+}) between the various solid phases and melt ($D_{Cr}^{ol/melt}$, etc.) in our experiments are shown as a function of $Cr\#_{sp}$ in Fig. 12a–d. Partition coefficients are approximately constant over the range of conditions of this study, regardless of whether the f_{O_2} values of the runs were buffered by Ru + RuO_2 or unbuffered, implying that most of the Cr in the solid phases of all experiments is Cr^{3+}. From these partition coefficients, the bulk distribution coefficient for a typical mantle peridotite under very oxidizing conditions ($D_{Cr^{3+}}^{residue/melt}$) would be about 5–10 (depending on the exact proportion of spinel at the solidus), confirming the highly compatible nature of Cr in its oxidized state. Liang & Elthon (1990) pointed out that the total Cr content of mantle peridotites does not change as a function of MgO content, where the latter is a proxy for melt extracted. This implies that $D_{\Sigma Cr}^{residue/melt}$ is ~1 during the mantle melting event from which these peridotites are the residue, and that therefore the Cr content of the melts must be similar to that in the primitive mantle, 2540 ppm (O'Neill & Palme, 1998), which is equivalent to 0·37 wt % 'Cr_2O_3'. Even if Sp ± Cpx were melted out, the value of $D_{Cr^{3+}}^{residue/melt}$ would drop only to a value intermediate between $D_{Cr}^{ol/melt}$ and $D_{Cr}^{opx/melt}$ for a harzburgite residue, which would still be >1, at least in the pressure regime of the spinel lherzolite facies. Moreover, this does not explain the flat trend of Cr vs MgO seen in the mantle peridotites. The discrepancy is likely to be due to Cr^{2+} in the melt during partial melting of the mantle, assuming that Cr^{2+} behaves moderately incompatibly. It is important to note that the presence of Cr^{2+} in the melt of an Fe-containing system does not require Cr^{2+} to be present in the solid phases, even if the system is closed to oxygen transfer, as Cr^{2+} may be produced from Cr^{3+} in the presence of Fe^{2+} by the electron exchange reaction $Cr^{3+} + Fe^{2+} = Cr^{2+} + Fe^{3+}$ (e.g. Berry *et al.*, 2001, 2003). However, in experimental simulations of mantle melting, which are in general open to oxygen (or at least imperfectly closed), this mechanism requires an oxygen fugacity regime in which just the right amount of Fe^{3+} is stable. Experiments conducted at lower f_{O_2} will produce more Cr^{2+} in the melt, depleting the residue in Cr^{3+}.

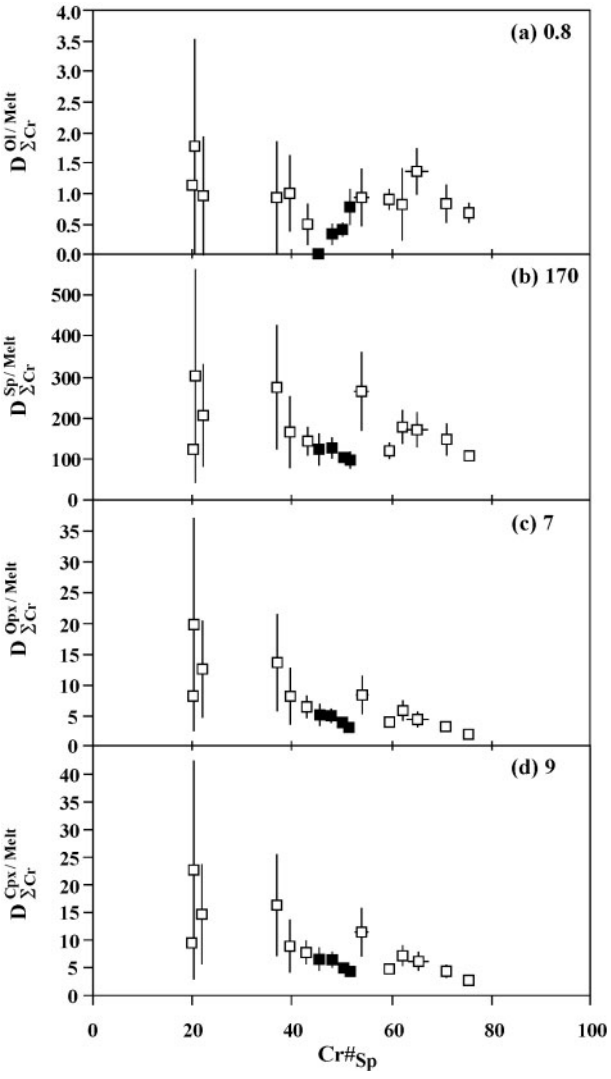

Fig. 12. The distribution of total Cr (ΣCr) vs $Cr\#_{sp}$ between Ol and melt (a), Sp and melt (b), Opx and melt (c), and Cpx and melt (d). The average values from all experiments are indicated. ■, experiments using Ru + RuO_2 buffer.

DISCUSSION

The effect of Cr_2O_3 on the lowering of Al_2O_3 in multiply saturated melt compositions

The dramatic decrease in Al_2O_3 with $Cr\#_{sp}$ for the multiply saturated melts in the system CMAS–Cr_2O_3 is entirely expected from equation (4). To illustrate this more quantitatively, let us consider the equilibrium

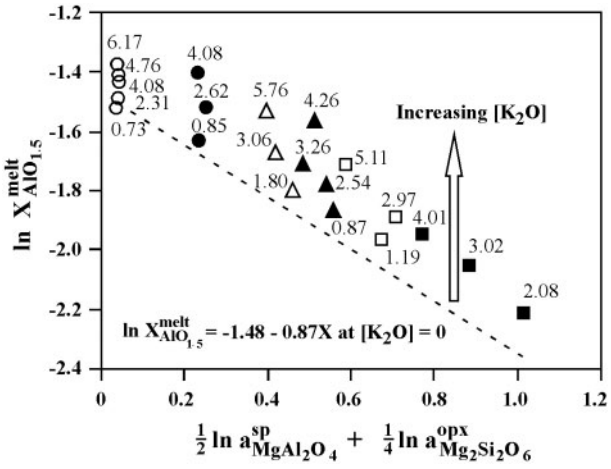

Fig. 13. Thermodynamic test of the effect of $Cr\#_{sp}$ on Al_2O_3 in multiply saturated melts. The dashed line is calculated for the system CMAS–Cr_2O_3 (i.e. K_2O-free) by first estimating the $Cr\#_{sp}$ at $[K_2O] = 0$ for every set of experiments, and then calculating the melt composition using the regression equations [equations (10)–(13) and (14)]; Opx compositions are taken from the experiments containing the lowest $[K_2O]$ at each $Cr\#_{sp}$. Thermodynamic models for Sp and Opx are from Klemme & O'Neill (2000). The small amount of CaO in Opx was ignored. The resulting line corresponds to the equation $\ln X^{melt}_{AlO_{1.5}} = -0{\cdot}87(\frac{1}{2}\ln a^{sp}_{MgAl_2O_4} + \frac{1}{4}\ln a^{opx}_{Mg_2Si_2O_6}) - 1{\cdot}48$. The theoretical slope should be approximately −1. The effect of increasing $[K_2O]$ is to increase $[AlO_{1.5}]$ in the melt.

constant for this reaction:

$$K = \frac{a^{melt}_{AlO_{1.5}} \left(a^{ol}_{Mg_2SiO_4}\right)^{1/2}}{\left(a^{sp}_{MgAl_2O_4}\right)^{1/2} \left(a^{opx}_{Mg_2Si_2O_6}\right)^{1/4}}. \qquad (15)$$

In Fig. 13, we plot $\ln X^{melt}_{AlO_{1.5}}$ vs $\frac{1}{2}\ln a^{sp}_{MgAl_2O_4} + \frac{1}{4}\ln a^{opx}_{Mg_2Si_2O_6}$ for all data from this study and those given by Liu & O'Neill (2004), for the melts multiply saturated in Ol + Sp + Opx + Cpx. We used the Opx and Sp models of Klemme & O'Neill (2000) to calculate $a^{sp}_{MgAl_2O_4}$ and $a^{opx}_{Mg_2Si_2O_6}$, and assumed $a^{ol}_{Mg_2SiO_4} = 1$. The stoichiometry of reaction (4) dictates that the data should plot on a line with a slope of −1 if they were isothermal, and if the activity coefficient of $AlO_{1.5}$ in the melt was constant. The line obtained by extrapolation of the melt compositions to $[K_2O] = 0$ is a fairly good approximation to that expected (slope −0·87), confirming that the change in melt composition is indeed mainly due to the lowering of the activity of Al_2O_3 in the system that the addition of Cr_2O_3 causes.

Multiple saturation and the CaO/Al_2O_3 ratio of primitive MORBs

The CaO/Al_2O_3 ratio of the Earth's mantle is the chondritic ratio of 0·79 (e.g. O'Neill & Palme, 1998). The commonest basaltic magmas coincidentally have a very similar ratio, e.g. primitive MORB has $CaO/Al_2O_3 = 0{\cdot}77 \pm 0{\cdot}05$ [mean and standard deviation of 42 glass analyses compiled by Presnall & Hoover (1987); see also Hess (1992)]. The mantle ratio is the Solar System ratio, whereas the basaltic ratio is controlled by phase equilibrium considerations [reactions (1) and (4) or (7)], hence the coincidence. Clearly, increasing the Cr_2O_3/Al_2O_3 ratio in a peridotitic system must result in a decrease in Al_2O_3 in the derived melt [reaction (4) or (7)], hence an elevation of CaO/Al_2O_3.

From a database of about 1700 analyses of abyssal basalt (MORB) glasses, Presnall & Hoover (1987) identified 42 primitive-looking compositions that they suggested were close to primary magma from the upper mantle. These primitive MORB glasses are shown in Fig. 14. They plot close to the melt composition produced at the multiply saturated spinel-lherzolite solidus in the system CMAS at 1·1 GPa, but in detail are dispersed along compositional 'vectors' appropriate to the effects of small amounts of Na_2O (<3 wt %), and $Cr\#_{sp}$ of between 30 and 40. The inferred range of Na_2O contents is consistent with that observed in the glasses (1·6–2·4 wt %). Considering that the effect of FeO as quantified recently by Gudfinnsson & Presnall (2000) on diagrams of this type is small, and that the other components in the primitive MORB glasses are negligible or almost so, the general conclusion is that the compositions of the primitive MORB glasses of Presnall & Hoover (1987) are indeed compatible with multiply saturated (Ol + Opx + Cpx ± Sp) melting of a peridotite source at an average pressure near 1·1 GPa, with Al_2O_3/Cr_2O_3 in the residue equivalent to that found in our experiments for $Cr\#_{sp}$ ~40. The amount of Cr_2O_3 in the melt at this $Cr\#_{sp}$ is ~0·2 wt % (Fig 11). This is rather more than observed in the primitive MORB glasses of Presnall & Hoover (1987), in which total 'Cr_2O_3' is ≤0·11 wt % (range 0–0·11 wt %), attesting to the probability of some low-pressure fractionation of Sp (± Ol) even in these primitive compositions.

Falloon *et al.* (1988) argued against the primitiveness of the MORB glasses assembled by Presnall & Hoover (1987) on the grounds of their high normative Di compared with the experimentally produced melt in equilibrium with a Sp-lherzolite (Fig. 15). This is because the experimental database available to Falloon *et al.* (1988) was biased towards systems with high Al_2O_3/Cr_2O_3. In part, this may be because the use of graphite capsules reduces much of the Cr^{3+} to Cr^{2+} in the melt. This explains the high 'Cr_2O_3' reported in melt compositions of Falloon *et al.* (1988), a point that those workers themselves acknowledged. As Fig. 14 shows, it is the Cr_2O_3 effect that accounts for the normative Di.

It is not clear if Sp is a solidus phase during melting of natural peridotite compositions. The Cr-rich spinel observed in residual peridotites could be a product of subsolidus re-equilibration [i.e. formed by Al_2O_3 and Cr_2O_3 from pyroxenes on cooling; see reaction (8)].

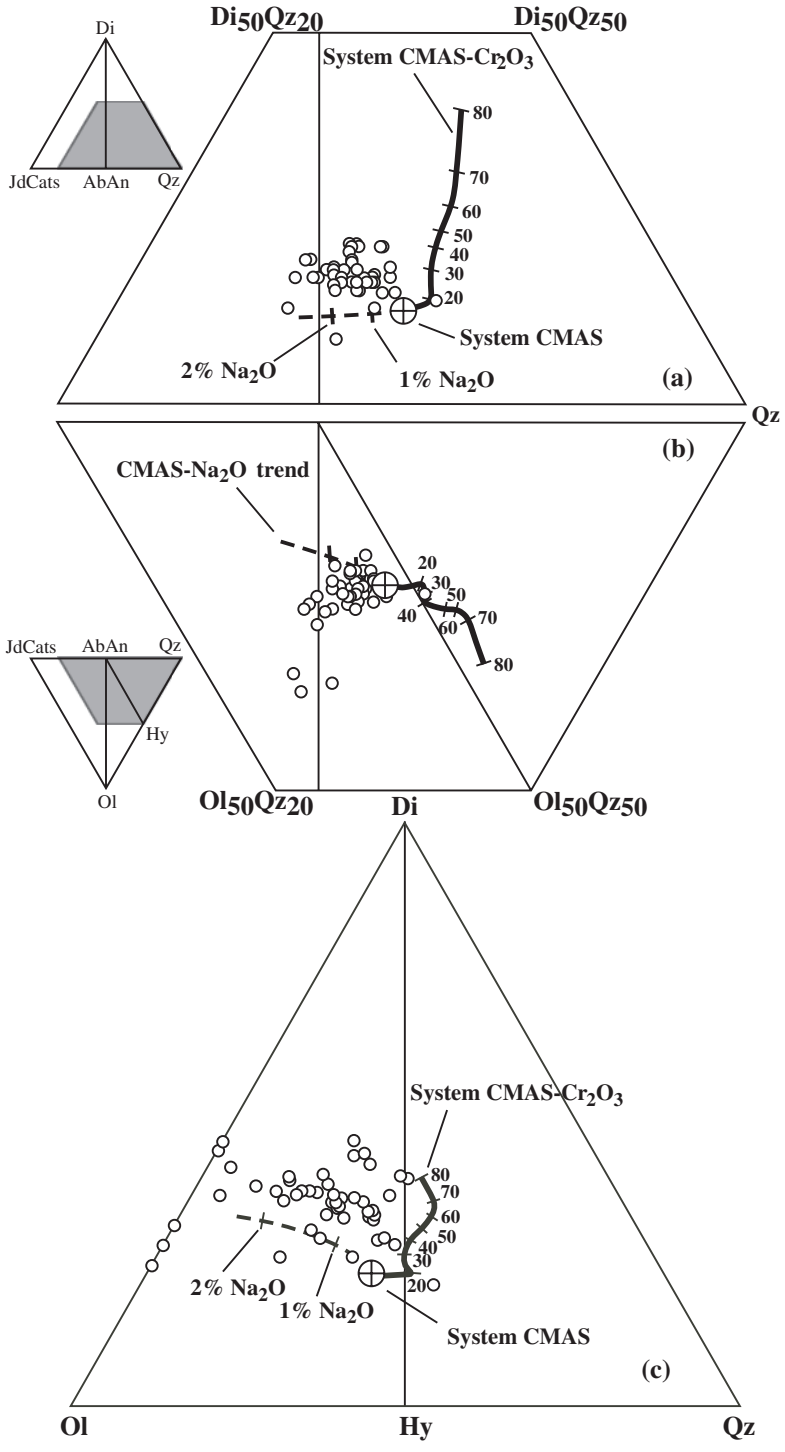

Fig. 14. Comparison of primitive MORB glasses from Presnall & Hoover (1987) with simple-system experimental data at 1·1 GPa. The solidus melt composition at the invariant point in the system CMAS is from Liu & O'Neill (2004); the near-solidus, multiply saturated melt in the system CMAS–Na_2O (dashed line, with Na_2O isopleths indicated in wt %) is from Liu (2003), and the melt in the system CMAS–Cr_2O_3 from this study (bold curve, contoured in $Cr\#_{sp}$). To a first approximation, the effects of Na_2O and $Cr\#_{sp}$ can be considered as compositional 'vectors' emanating from the CMAS invariant point. The effect of other compositional variables (FeO, TiO_2, volatiles) and of pressure could be represented by similar 'vectors'; those for pressure are shown in Fig. 6. The net effect of all such variables will be to increase the scatter of the data. Given this complexity, the major-element chemistry of most of the primitive MORB glasses of Presnall & Hoover (1987) appears to be consistent with equilibrium, multiply saturated (Ol + Opx + Cpx ± Sp), batch partial melts of likely mantle perididitite compositions near 1·1 GPa, with Cr_2O_3/Al_2O_3 in the residue equivalent to $Cr\#_{sp}$ of 30–40.

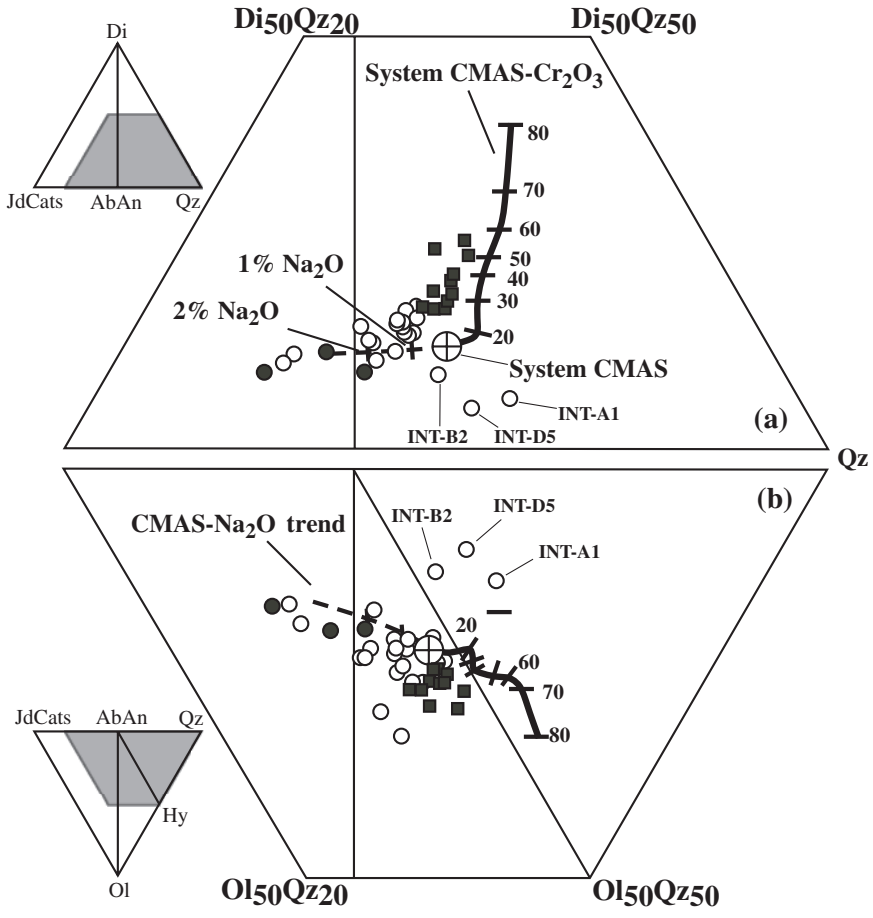

Fig. 15. Multiply saturated (Ol + Opx + Cpx + Sp) melts from experiments on natural peridotite compositions compared with melts in the systems CMAS, CMAS–Na_2O and CMAS–Cr_2O_3 (see Fig. 14). Experimental data for the complex compositions are from Baker & Stolper (1994), Falloon *et al.* (1999, 2001), Pickering-Witter & Johnston (2000) and Schwab & Johnston (2001). The experimental pressure in all these studies is 1·0 GPa. •, $Cr\#_{sp}$ 0–20; ○, $Cr\#_{sp}$ 30–45; ■, $Cr\#_{sp}$ >40. Three apparently anomalous points from Schwab & Johnston (2001) at very low melt fractions (2·4, 0·1 and 1·4 wt %) are identified.

The presence of Cr-rich spinel in experiments is heavily dependent on oxygen fugacity because of the role of Cr^{2+} and is a poor guide. The effect of undersaturation in Sp would be to lower further the activity of Al_2O_3 in the melt [reaction (4)], thus exaggerating the increase in normative Di and associated compositional changes. We emphasize again that the Cr_2O_3 effect is not dependent on the presence of Sp, but having Sp in our experiments provides a ready means of characterizing the Al_2O_3/Cr_2O_3 activity ratio through $Cr\#_{sp}$.

Melt inclusions with high CaO/Al_2O_3 ratios

Recent studies of melt inclusions in phenocrysts from mid-ocean ridge (Kamenetsky, 1996; Kamenetsky & Crawford, 1998; Kamenetsky *et al.*, 1998; Sours-Page *et al.*, 1999), volcanic arc (Schiano *et al.*, 2000), back-arc basin (Kamenetsky *et al.*, 1997) and oceanic island settings (Sigurdsson *et al.*, 2000; Slater *et al.*, 2001) have documented glasses with unusually high CaO/Al_2O_3 ratios (up to 1·77; Kogiso & Hirschmann, 2001). High CaO/Al_2O_3 compositions have also been found in lavas from some volcanic arcs (Barsdell, 1988; Barsdell & Berry, 1990). Generally the high CaO/Al_2O_3 melts can be subdivided into two groups: SiO_2-poor nepheline-normative compositions from volcanic arcs and SiO_2-rich Hy-normative compositions from all other localities. The latter show a trend almost parallel to the CMAS–Cr_2O_3 trend of this study (Fig. 16), displaced somewhat along a Na_2O 'vector', appropriate for their observed Na_2O contents of 1–2 wt %. The former group of melts exhibits a very different trend, and these melts will not be considered further here.

Kogiso & Hirschmann (2001) showed from a direct experimental study of the partial melting of three clinopyroxenite compositions that although several features of the Hy-normative high CaO/Al_2O_3 compositions could be reproduced, this was only at very high melt fractions and temperatures much higher than the peridotite

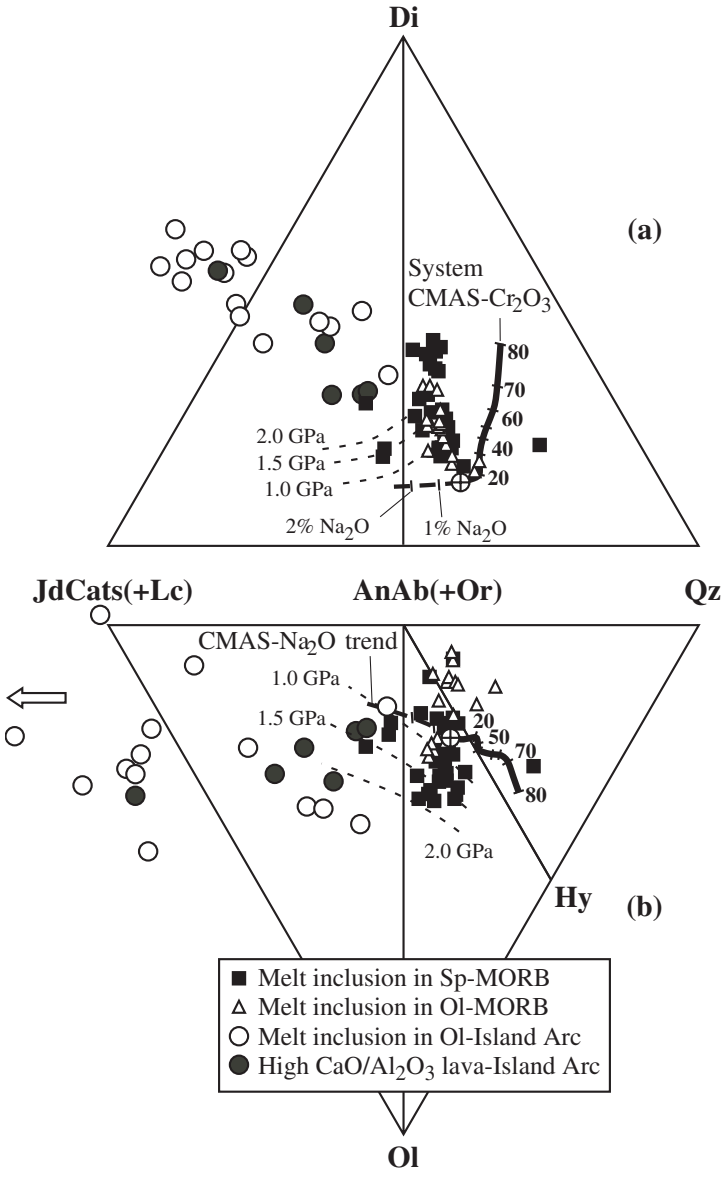

Fig. 16. Comparison of high CaO/Al_2O_3 natural melt inclusions with near-solidus melts in the systems CMAS, CMAS–Na_2O and CMAS–Cr_2O_3 (see Fig. 13). Melt inclusions in Sp (MORB or OIB) are from Donaldson & Brown (1977), Kamenetsky (1996), Kamenetsky & Crawford (1998), Kamenetsky *et al.* (1998, 2001) and Sigurdsson *et al.* (2000). Melt inclusions in Ol in MORB are from Danyushevsky *et al.* (1987), Kamenetsky & Crawford (1998) and Kamenetsky *et al.* (1998), and melt inclusions in Ol (plus some similar lava compositions) in island-arc basalts (IAB) are from Schiano *et al.* (2000; Tables 1 and 2). In all cases host Ol has mg# $\geq$89. The arrow in (b) indicates some IAB with extreme melt compositions. The trapping pressures of the melt inclusions are unknown. The cotectics of Ol + Opx + Cpx ± Sp at 1·0, 1·5 and 2·0 GPa shown as fine dashed curves are for pyrolite (Green & Falloon, 1998).

solidus. They suggested that partial melting of a depleted harzburgite might be important in the genesis of these unusual melts. Our study supports this conclusion.

It may not be intuitively obvious why high CaO/Al_2O_3 melts could be produced from depleted sources poor or even lacking in the main CaO-containing phase, Cpx, but the reason is as follows. The strong decrease in Al_2O_3 in the melt caused by decreasing Al_2O_3/Cr_2O_3 in the residue (Fig. 5b) causes the CaO/Al_2O_3 of the melt to increase from $\sim$0·7 at $Cr\#_{sp} = 0$ to $\sim$1·7 at $Cr\#_{sp} = 75$ (Fig. 17). However, the activity of CaO remains buffered at a constant value until Cpx is completely exhausted in the residue [reaction (1)]. As discussed above, the SiO_2 content and the Hy component of the melt also increase with $Cr\#_{sp}$. It follows that the SiO_2-rich, Hy-normative and high CaO/Al_2O_3 melt inclusions shown in Fig. 16 can be explained by a low Al_2O_3/Cr_2O_3 ratio, rather than modal abundance of Cpx; low Al_2O_3/Cr_2O_3 is an

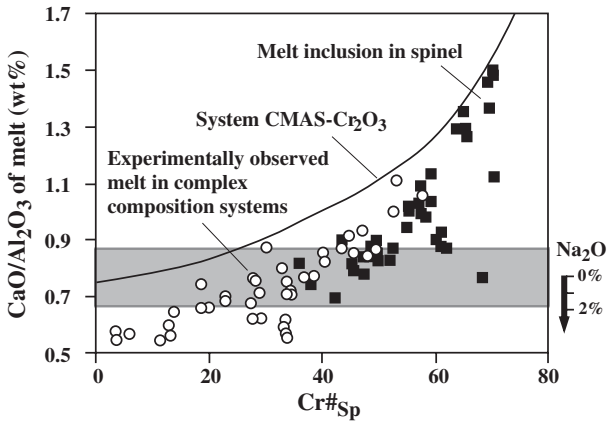

Fig. 17. The relationship between CaO/Al_2O_3 ratio of multiply saturated melts and $Cr\#_{sp}$. Experimental data for natural composition systems are from Baker & Stolper (1994), Robinson *et al.* (1998), Falloon *et al.* (1999, 2001), Pickering-Witter & Johnston (2000) and Schwab & Johnston (2001). The pressure in all these experimental studies is 1·0 GPa, except for the Robinson *et al.* (1998) study (1·5 GPa). Melt inclusions in Sp are from either mid-ocean ridge or ocean island basalts (for data sources, see the caption to Fig. 15). The shaded area represents ±2 SD of the mean CaO/Al_2O_3 of the primitive MORB glasses from Presnall & Hoover (1987). The experimental and natural data fall below the curve for CMAS–Cr_2O_3 because of the effect of Na_2O.

obvious consequence of depletion of the source peridotite by previous melt extraction, given that Al_2O_3 is incompatible whereas Cr_2O_3 is compatible.

In Fig. 17 we also plot the CaO/Al_2O_3 ratio of experimental multiply saturated melts in systems with natural lherzolitic compositions. As a result of the presence of Na_2O, the CaO/Al_2O_3 ratio of the melt produced by the natural systems at low degrees of melting (i.e. multiply saturated by Ol + Opx + Cpx ± Sp) is always lower than that in the system CMAS–Cr_2O_3.

The SiO_2-rich, Hy-normative and high CaO/Al_2O_3 melt inclusions hosted in spinel are also shown in Fig. 17. Remarkably, the CaO/Al_2O_3 of the melt inclusions are very similar to the experimental melts from the natural peridotitic compositions at similar Cr_2O_3 activity (which is indicated by $Cr\#_{sp}$). The implication is that these melt inclusions are indeed produced from previously depleted sources.

The range of CaO/Al_2O_3 in the primitive MORB glasses is also shown in Fig. 17. The CaO/Al_2O_3 of these glasses corresponds to $Cr\#_{sp} = 40 \pm 10$, in good agreement with the conclusions from the projections of the glasses compared with our experiments shown in Fig. 14.

The effect of pressure on the behaviour of Cr_2O_3

The behaviour of Cr_2O_3 in peridotites depends on the pressure. In the spinel lherzolite facies, Cr_2O_3 substitutes for Al_2O_3 in spinel and pyroxenes, and thus has a great effect on the activity of Al_2O_3 in the system. As it plays an essential role in the stoichiometry of these phases, Cr_2O_3 belies its modest abundance in peridotite systems by behaving as a major-element component in the spinel lherzolite facies, according to the distinction between major and trace elements introduced by Hanson & Langmuir (1978). Now, at lower pressures where plagioclase becomes stable, the activity of Al_2O_3 in the system is given by reaction (5). Because Cr^{3+} does not substitute significantly for the tetrahedrally coordinated Al in plagioclase, the control on the activity of Al_2O_3 from reaction (5) would appear, at first sight, to be independent of the amount of Cr_2O_3 in the system. However, the presence or absence of plagioclase at any given pressure is itself dependent on the Cr^{3+}/Al ratio of the system [reaction (6)]. At very low pressures, Cr_2O_3 does not behave so much like a major-element component, but a minor element that forms its own accessory phase (that is, chromite), rather like Zr forming zircon or S forming sulfide. Thus the Cr_2O_3 effect described in this paper has a negligible influence on 1 atm phase relations [as shown directly by Libourel (1991)].

At higher pressures, garnet becomes stable in place of spinel in mantle peridotite, and the activity of Al_2O_3 is given by

$$\underset{\text{Melt}}{AlO_{1.5}} + 0{\cdot}75\underset{\text{Opx}}{Mg_2Si_2O_6} = 0{\cdot}5\underset{\text{Gt}}{Mg_3Al_2Si_3O_{12}}. \quad (16)$$

The influence of Cr_2O_3 on the activity of the aluminous component in garnet, $Mg_3Al_2Si_3O_{12}$, is much less than the corresponding influence on the activity of $MgAl_2O_4$ in spinel at lower pressures, both because of the relative instability of Cr^{3+}-containing garnet components such as $Mg_3Cr_2Si_3O_{12}$, but also because the solubility of Al_2O_3 in pyroxenes decreases with increasing pressure in the garnet stability field, concentrating Al_2O_3 in garnet. Hence at higher pressures the effect of Cr_2O_3 on the activity of Al_2O_3, although not negligible, tends to become less significant, and the behaviour of Cr becomes more like that of a trace element.

There is nothing anomalous in all this: the transitions in these contrasting styles of behaviour are smoothed out by the effect that Cr_2O_3 has on the phase boundaries between both plagioclase lherzolite and spinel lherzolite, and spinel lherzolite and garnet lherzolite (e.g. O'Neill, 1981). However, the important point is that the Cr effect as described in this study has its maximum influence in the pressure regime where spinel lherzolite is stable; this is also the pressure regime in which the common basalts probably mostly originate.

It is interesting to compare the behaviour of Cr_2O_3 with Na_2O during mantle melting. Both are present in the primitive mantle at similar levels (0·37 wt % Cr_2O_3, 0·35 wt % Na_2O; O'Neill & Palme, 1998). As shown in

this study, their influences on melt composition are comparable in magnitude (see Fig. 14). The obvious contrast is that Na_2O is an incompatible component that exerts its influence on the partial melting equilibrium through its concentration in the melt, whereas Cr_2O_3, being highly compatible, exerts its influence through the properties of the residue. Thus Na_2O is recognized as a major-element component in basalt generation, whereas Cr_2O_3 has hitherto not been. Interestingly, both components have their maximum effect in the pressure regime of the spinel lherzolite facies, as Na_2O becomes more compatible in its behaviour at lower pressures when plagioclase is present, or at higher pressures owing to the increasing stability of the $NaAlSi_2O_6$ (Jd) component in Cpx.

Implications for the 'inverse approach' in experimental petrology

In experimental petrology, the investigation of the origins of basalts has historically used two approaches, 'forward' and 'inverse'. In the 'forward approach', an assumed bulk composition is partially melted, and the resulting phase compositions, including the melt composition, are determined. This is the approach used in this study. One perceived problem with this approach is that the bulk composition of the system must be assumed, whereas in many situations, particularly for extraterrestrial basalts, it is only the composition of the derived partial melt (i.e. the erupted basalt) that is known, or, more truthfully, thought to be known—this raises the issue of whether 'primary magmas', which are defined as magmas sampled at the Earth's surface having undergone minimal low-pressure crystal fractionation, really exist. This is controversial (e.g. Herzberg & O'Hara, 1998). Nevertheless, a theoretical 'primary magma' composition might in principle be reconstructed.

The 'inverse approach' takes the existence of a suitable primary magma composition as a given, and then seeks to ascertain the conditions under which it was produced by examining its crystallization behaviour as a function of pressure, temperature and other pertinent variables such as volatile content and redox state.

Some potential problems with the 'inverse approach' have been discussed by Hess (1989; pp. 109–113) and more recently by Falloon *et al.* (1999). Here we add another fundamental item to these critiques, deriving from the behaviour of Cr_2O_3 during partial melting.

The basic assumption underlying the 'inverse approach' is that all the information needed to reconstruct the partial melting equilibrium is held in the melt composition. Heuristically, this would not be true were there a component of the system that was perfectly refractory, such that it entered only the solid phases of the partial melting equilibrium and not the melt. The concentration of such a component in the system could not be determined from the melt, but its presence in the solid phases would affect the chemical potentials of other components in the system, and hence their concentrations in the melt. Although Cr_2O_3 is not quite perfectly refractory, its highly compatible behaviour is as near to this as makes no practical difference. Although Cr_2O_3 does enter the melt, the amount is so small that it is commonly overlooked, and the role of Cr_2O_3 as a major-element component during basalt generation has tended to go unrecognized. Even once its importance is acknowledged, it is doubtful if accurate primary Cr contents could be deduced, as Cr-rich spinel is commonly the first phase to fractionate from a magma at low pressures, easily obscuring original Cr. Thus the primitive MORB glasses of Presnall & Hoover (1987) contain only 0–0·11 wt % total 'Cr_2O_3', whereas, as we have argued above, the amount of Cr_2O_3 (i.e. Cr as Cr^{3+} only) expected from the compositions of these melts is ~0·2 wt %. The amount of 'Cr_2O_3' in primitive melts inferred from the flat trend of Cr_2O_3 vs MgO in residual peridotites is 0·37 wt % (Liang & Elthon, 1990; O'Neill & Palme, 1998).

Furthermore, the compatible behaviour of interest here is specifically a property of Cr^{3+} and not Cr^{2+}, hence the proportion of total Cr as Cr^{3+} in the melt is what matters. This depends on the redox state of the system, i.e. the Fe^{3+}/Fe^{2+} ratio of the melt, T and P. In natural Fe-rich compositions the original Cr^{3+}/Cr^{2+} ratios are modified during cooling or crystallization by the electronic exchange reaction $Cr^{2+} + Fe^{3+} = Cr^{3+} + Fe^{2+}$. This reaction proceeds to the right-hand side with cooling or crystallization (e.g. Berry *et al.*, 2001, 2003); under terrestrial conditions there is always enough Fe^{3+} in natural compositions to consume completely the Cr^{2+} present originally at magmatic temperatures. To summarize: the compositions of partial melts from mantle peridotite depend on the activity of Cr_2O_3 in the residue, and this is not practicably ascertainable from analysing Cr in the melt.

Any composition identified as 'primary' (for example, on the usual grounds of high MgO and the appropriate Mg/Fe^{2+} ratio to be in equilibrium with olivine of $Fo_{89–92}$) would also have to have exactly the right Cr^{3+} content to reproduce the partial melting equilibrium; as we have pointed out, this is in practice hardly possible to achieve. Accordingly, the fundamental assumption of the 'inverse approach', that all the necessary information is held in the melt composition, is not valid. For example, the 'inverse approach' has been used to test whether a magma composition is primary by seeing whether it becomes multiply saturated with Ol + Opx + Cpx at some pressure. As Fig. 6 shows, this requires exact knowledge of the Cr_2O_3 activity in the residue. Similarly, inferences regarding the depth of origin of a primary magma from experimental multiple saturation would be

sustainable only if the Opx ± Cpx crystallizing in the experiment can be shown to have the appropriate compositions, including Cr and Al contents, which necessarily requires detailed knowledge of the source.

The large amount of effort expended by experimental petrologists on the 'inverse approach' should not be seen as wasted, however. 'Inverse' experiments are a good means of obtaining the phase equilibrium data needed to formulate models for calculating melting phenomena under physically plausible conditions. In many ways, the simplified answers sought originally from the 'inverse approach', such as the depth of melting, have become irrelevant as the physical context of partial melting has become better understood. Basaltic magmas are now recognized as being mostly, perhaps exclusively, produced by convective upwelling in the mantle, with partial melting occurring under nearly adiabatic conditions, and over an interval of pressure (e.g. McKenzie & Bickle, 1988). Melts are extracted more-or-less fractionally, resulting in changing bulk compositions during the melting process. The mantle may also act as an open system (e.g. to volatile components). These complex natural processes cannot be mimicked in the laboratory with any expectation that accurate phase equilibrium data will result. Carrying out polybaric, adiabatic melting experiments is just too difficult. As for any complex natural process, the path that modern science must take to escape this dilemma is to construct a computer model for the phase equilibria that will allow this aspect of the partial melting process to be integrated into a holistic description of the whole process. Such models are being developed, notably the MELTS algorithm (e.g. Ghiorso *et al.*, 2002) and similar parameterizations (e.g. Walter *et al.*, 1995; Herzberg & O'Hara, 2002). The experimental petrology of basalt generation should now appropriately be directed towards the goal of supplying the necessary phase equilibrium information to improve these models.

ACKNOWLEDGEMENTS

We gratefully acknowledge the technical assistance of Bill Hibberson, Dean Scott, Nick Ware, Mike Shelley, Frank Brink, Dr Roger Heady and Dr Cheng Huang. We benefited from constructive discussions with Professors David Green, Max Schmidt and Jianping Li, and Drs Sue Kesson, Jörg Hermann and Stephen Eggins. Dr Leonid Danyushevsky and an anonymous reviewer are thanked for their extensive and detailed reviews, and Professor Richard Arculus for his editorial handling. This study is part of the Ph.D. thesis of L.X. funded by an A. E. Ringwood Memorial Scholarship and an Australian International Postgraduate Research Scholarship. L.X. also thanks Dr Shen-su Sun and Professors Qingchen Wang and Lifei Zhang for their encouragement.

REFERENCES

Baker, M. B. & Stolper, E. M. (1994). Determining the composition of high-pressure mantle melts using diamond aggregates. *Geochimica et Cosmochimica Acta* **58**, 2811–2827.

Barnes, S. J. & Roeder, P. L. (2001). The range of spinel compositions in terrestrial mafic and ultramafic rocks. *Journal of Petrology* **42**, 2279–2302.

Barsdell, M. (1988). Petrology and petrogenesis of clinopyroxene-rich tholeiitic lavas, Merelava volcano, Vanuatu. *Journal of Petrology* **29**, 927–964.

Barsdell, M. & Berry, R. F. (1990). Origin and evolution of primitive island arc ankaramites from Western Epi, Vanuatu. *Journal of Petrology* **31**, 747–777.

Berry, A. J., O'Neill, H. St. C., Shelley, J. M. G. & Foran, G. (2001). Spectroscopic evidence for chromium (II) in silicate melts. In: *Eleventh Annual V. M. Goldschmidt Conference. Lunar and Planetary Institute Contribution* **1088**, Abstract 3566.

Berry, A. J., Shelley, J. M. G., Foran, G. J., O'Neill, H. St. C. & Scott, D. R. (2003). A furnace design for XANES spectroscopy of silicate melts under controlled oxygen fugacities and temperatures up to 1773 K. *Journal of Synchrotron Radiation* **10**, 332–336.

Brey, G. P. & Kohler, T. (1990). Geothermobarometry in four-phase lherzolite II: new thermobarometers, and practical assessment of existing thermobarometers. *Journal of Petrology* **31**, 1353–1378.

Brey, G. P., Kohler, T. & Nickel, K. G. (1990). Geothermobarometry in four-phase lherzolites I. Experimental results from 10 to 60 kb. *Journal of Petrology* **31**, 1313–1352.

Danyushesky, L. V., Sobolev, A. V. & Dmitriev, L. V. (1987). Low-titanium orthopyroxene-bearing tholeiite, a new type of ocean-rift tholeiite. *Transactions (Doklady) of the USSR Academy of Sciences* **292**, 102–105.

Dick, H. J. B. & Bullen, T. (1984). Chromian spinel as a petrogenetic indicator in abyssal and alpine-type peridotites and spatially associated lavas. *Contributions to Mineralogy and Petrology* **86**, 54–76.

Donaldson, C. H. & Brown, R. W. (1977). Refractory megacrysts and magnesium-rich melt inclusions within spinel in oceanic tholeiites: indicators of magma mixing and parental magma compositions. *Earth and Planetary Science Letters* **37**, 81–89.

Dunn, R. & Forsyth, D. (2001). Short-period Love waves reveal the transition from broad mantle upwelling to the narrow crustal magmatic system beneath the southern East Pacific Rise. *EOS Transactions, American Geophysical Union* **82**, 1113.

Falloon, T. J. & Green, D. H. (1987). Anhydrous partial melting of MORB pyrolite and other peridotite compositions at 10 kbar: implications for the origin of MORB glasses. *Mineralogy and Petrology* **37**, 181–219.

Falloon, T. J. & Green, D. H. (1988). Anhydrous partial melting of peridotite from 8 to 35 kbars and the petrogenesis of MORB. *Journal of Petrology, Special Issue*, 379–414.

Falloon, T. J., Green, D. H., Hatton, C. J. & Harris, K. L. (1988). Anhydrous partial melting of a fertile and depleted peridotite from 2 to 30 kbar and application to basalt petrogenesis. *Journal of Petrology* **29**, 1257–1282.

Falloon, T. J., Green, D. H., Danyushevsky, L. V. & Faul, U. H. (1999). Peridotite melting at 1·0 and 1·5 GPa: an experimental evaluation of techniques using diamond aggregates and mineral mixes for determination of near-solidus melts. *Journal of Petrology* **40**, 1343–1375.

Falloon, T. J., Danyushevsky, L. V. & Green, D. H. (2001). Peridotite melting at 1 GPa: reversal experiments on partial melt compositions produced by peridotite–basalt sandwich experiments. *Journal of Petrology* **42**, 2363–2390.

Ford, C. E., Russell, D. G., Graven, J. A. & Fisk, M. R. (1983). Olivine–liquid equilibria: temperature, pressure and composition dependence of the crystal/liquid cation partition coefficients for Mg, Fe^{2+}, Ca and Mn. *Journal of Petrology* **24**, 256–265.

Gasparik, T. (1984). Two-pyroxene thermobarometry with new experiment data in the system CaO–MgO–Al_2O_3–SiO_2. *Contributions to Mineralogy and Petrology* **87**, 87–97.

Ghiorso, M. S., Hirschmann, M. M., Reiners, P. W. & Kress, V. C. (2002). The pMELTS: a revision of MELTS for improved calculation of phase relations and major element partitioning related to partial melting of the mantle to 3 GPa. *Geochemistry, Geophysics, Geosystems* **3**, 2001GC000217.

Girnis, A. V., Brey, G. P., Doroshev, A. M., Turkin, A. I. & Simon, N. (2003). The system MgO–Al_2O_3–SiO_2–Cr_2O_3 revisited: reanalysis of Doroshev *et al.*'s (1997) experiments and new experiments. *European Journal of Mineralogy* **15**, 953–964.

Green, D. H. & Falloon, T. J. (1998). Pyrolite: a Ringwood concept and its current expression. In: Jackson, I. (ed.) *The Earth's Mantle: its Origin, Structure and Evolution*. Cambridge: Cambridge University Press, pp. 311–378.

Gudfinnsson, G. H. & Presnall, D. C. (1996). Melting relations of model lherzolite in the system CaO–MgO–Al_2O_3–SiO_2 at 2·4–3·4 GPa and the generation of komatiites. *Journal of Geophysical Research* **101**, 27701–27709.

Gudfinnsson, G. H. & Presnall, D. C. (2000). Melting behaviour of model lherzolite in the system CaO–MgO–Al_2O_3–SiO_2–FeO at 0·7–2·8 GPa. *Journal of Petrology* **41**, 1241–1269.

Hanson, G. N. & Langmuir, C. H. (1978). Modelling of major elements in mantle–melt systems using trace element approaches. *Geochimica et Cosmochimica Acta* **42**, 725–741.

Herzberg, C. T. & O'Hara, M. J. (1998). Phase equilibrium constraints on the origin of basalts, picrites, and komatiites. *Earth-Science Reviews* **44**, 39–79.

Herzberg, C. T. & O'Hara, M. J. (2002). Plume-associated ultramafic magmas of Phanerozoic age. *Journal of Petrology* **43**, 1857–1883.

Hess, P. C. (1989). *Origins of Igneous Rocks*. Cambridge, MA: Harvard Press.

Hess, P. C. (1992). Phase equilibria constraints on the origin of ocean floor basalts. In: Phipps Morgan, J., Blackman, D. & Sinton, J. (eds) *Mantle Flow and Melt Generation at Mid-ocean Ridge. Geophysical Monograph, American Geophysical Union* **71**, 67–102.

Irvine, T. N. (1977). Chromite crystallisation on the join Mg_2SiO_4–$CaMgSi_2O_6$–$CaAl_2Si_2O_8$–$MgCr_2O_4$–SiO_2. *Carnegie Institution of Washington Yearbook* **76**, 465–472.

Jochum, K. P., Dingwell, D. B., Rocholl, A., *et al.* (2000). The preparation and preliminary characterisation of eight geological MPI-DING reference glasses for in-situ microanalysis. *Journal of Geostandards and Geoanalysis* **24**, 87–133.

Kamenetsky, V. S. (1996). Methodology for the study of melt inclusions in Cr-spinel, and implications for parental melts of MORB from FAMOUS area. *Earth and Planetary Science Letters* **142**, 479–486.

Kamenetsky, V. S. & Crawford, A. J. (1998). Melt–peridotite reaction recorded in the chemistry of spinel and melt inclusions in basalt from 43°N, Mid-Atlantic Ridge. *Earth and Planetary Science Letters* **164**, 345–352.

Kamenetsky, V. S., Crawford, A. J., Eggins, S. M. & Muhe, R. (1997). Phenocrysts and melt inclusion chemistry of near-axis seamounts, Valu Fa Ridge, Lau Basin: insight into mantle wedge melting and the addition of subduction components. *Earth and Planetary Science Letters* **151**, 205–223.

Kamenetsky, V. S., Eggins, S. M., Crawford, A. J., Green, D. H., Gasparon, M. & Falloon, T. J. (1998). Calcic melt inclusions in primitive olivine at 43°N MAR: evidence for melt-rock reaction/melting involving clinopyroxene-rich lithologies during MORB generation. *Earth and Planetary Science Letters* **160**, 115–132.

Kamenetsky, V. S., Crawford, A. J. & Meffre, S. (2001). Factors controlling chemistry of magmatic spinel: an empirical study of associated olivine, Cr-spinel and melt inclusions from primitive rocks. *Journal of Petrology* **42**, 655–671.

Klemme, S. & O'Neill, H. St. C. (2000). The effect of Cr on the solubility of Al in orthopyroxene: experiments and thermodynamic modelling. *Contributions to Mineralogy and Petrology* **140**, 84–98.

Kogiso, T. & Hirschmann, M. M. (2001). Experimental study of clinopyroxenite partial melting and the origin of ultra-calcic melt inclusions. *Contributions to Mineralogy and Petrology* **142**, 347–360.

Li, J. P., O'Neill, H. St. C. & Seifert, F. (1995). Subsolidus phase relations in the system MgO–SiO_2–Cr–O in equilibrium with metallic Cr, and their significance for the petrochemistry of chromium. *Journal of Petrology* **36**, 107–132.

Liang, Y. & Elthon, D. (1990). Evidence from chromium abundances in mantle rocks for extraction of picrite and komatiite melts. *Nature* **343**, 551–553.

Libourel, G. (1991). Chromium in basalts: an experimental study. *EOS Transactions, American Geophysical Union* **72**, 547.

Lindsley, D. H. & Dixon, S. A. (1976). Diopside–enstatite equilibria at 850 to 1400°C, 5 to 35 kbar. *American Journal of Science* **276**, 1285–1301.

Liu, X. (2003). Effect of K_2O, Cr_2O_3, H_2O and CO_2 on the partial melting behaviour of spinel lherzolite in system CaO–MgO–Al_2O_3–SiO_2 ± K_2O ± Cr_2O_3 ± H_2O ± CO_2 at 11 kbar. Ph.D. thesis, Australian National University, Canberra.

Liu, X. & O'Neill, H. St.C. (2004). Partial melting of spinel lherzolite in the system CaO–MgO–Al_2O_3–SiO_2 ± K_2O at 1·1 GPa. *Journal of Petrology* **45**, 1339–1368.

Longhi, J. (1987). Liquidus equilibria and solid solution in the system $CaAl_2Si_2O_8$–Mg_2SiO_4–$CaSiO_3$–SiO_2 at low pressure. *American Journal of Science* **287**, 265–331.

Longhi, J. & Bertka, C. M. (1996). Graphical analysis of pigeonite–augite liquidus equilibria. *American Mineralogist* **81**, 685–695.

McKenzie, D. & Bickle, M. J. (1988). The volume and composition of melt generated by extension of the lithosphere. *Journal of Petrology* **29**, 625–679.

Melt Seismic Team (1998). Imaging the deep seismic structure beneath a mid-ocean ridge: the melt experiment. *Science* **280**, 1215–1218.

Mori, T. & Green, D. H. (1976). Subsolidus equilibria between pyroxenes in the CaO–MgO–SiO_2 system at high pressures and temperatures. *American Mineralogist* **61**, 616–625.

Nagata, J., Goto, A. & Obata, M. (1983). The parabolic pattern of chromium partitioning observed between pyroxenes and spinel from ultramafic rocks and its petrologic significance. *Contributions to Mineralogy and Petrology* **82**, 42–51.

Nickel, K. G. (1986). Phase equilibria in the system SiO_2–MgO–Al_2O_3–CaO–Cr_2O_3 (SMACCr) and their bearing on spinel/garnet lherzolite relationships. *Neues Jahrbuch für Minerologie, Abhandlungen* **155**, 259–287.

Nickel, K. G. & Brey, G. P. (1984). Subsolidus orthopyroxene–clinopyroxene systematics in the system CaO–MgO–SiO_2 to 60 kb: a re-evaluation of the regular solution model. *Contributions to Mineralogy and Petrology* **87**, 35–42.

Nickel, K. G., Brey, G. P. & Kogarto, L. (1985). Orthopyroxene–clinopyroxene equilibria in the system CaO–MgO–Al_2O_3–SiO_2. *Contributions to Mineralogy and Petrology* **91**, 44–53.

O'Neill, H. St. C. (1981). The transition between spinel lherzolite and garnet lherzolite, and its use as a geobarometer. *Contributions to Mineralogy and Petrology* **77**, 185–194.

O'Neill, H. St. C. & Nell, J. (1997). Gibbs free energies of formation of RuO_2, IrO_2, and OsO_2: a high-temperature electrochemical and calorimetric study. *Geochimica et Cosmochimica Acta* **61**, 5279–5293.

O'Neill, H. St. C. & Palme, H. (1998). Compositions of the Silicate Earth: implications for accretion and core formation. In: Jackson, I. (ed.) *The Earth's Mantle: Composition, Structure and Evolution*. Cambridge: Cambridge University Press, pp. 3–126.

Pickering-Witter, J. W. & Johnston, A. D. (2000). The effects of variable bulk composition on the melting systematics of fertile peridotitic assemblages. *Contributions to Mineralogy and Petrology* **140**, 190–211.

Presnall, D. C. & Hoover, J. D. (1984). Composition and depth of origin of primary mid-ocean ridge basalts. *Contributions to Mineralogy and Petrology* **87**, 170–178.

Presnall, D. C. & Hoover, J. D. (1987). High pressure phase equilibrium constraints on the origin of mid-ocean ridge basalts. In: Mysen, B. O. (ed.) *Magmatic Processes: Physicochemical Principles*. *Geochemical Society, Special Publication* **1**, 75–89.

Presnall, D. C., Dixon, J. R., O'Donnell, T. H. & Dixon, S. A. (1979). Generation of mid-ocean ridge tholeiites. *Journal of Petrology* **20**, 3–36.

Presnall, D. D., Gudfinnsson, G. H. & Walter, M. J. (2002). Generation of mid-ocean ridge basalts at pressures from 1 to 7 GPa. *Geochimica et Cosmochimica Acta* **66**, 2073–2090.

Robinson, J. A. C., Wood, B. J. & Blundy, J. D. (1998). The beginning of melting of fertile and depleted peridotite at 1·5 GPa. *Earth and Planetary Science Letters* **155**, 97–111.

Schiano, P., Eiler, J. M., Hutcheon, I. D. & Stolper, E. M. (2000). Primitive CaO-rich, silica-undersaturated melts in island arcs: evidence for the involvement of clinopyroxene-rich lithologies in the petrogenesis of arc magmas. *Geochemistry, Geophysics, Geosystems* **1**, 1999GC000032.

Schwab, B. E. & Johnston, A. D. (2001). Melting systematics of modally variable, compositionally intermediate peridotites and the effects of mineral fertility. *Journal of Petrology* **42**, 1789–1811.

Sen, G. (1982). Composition of basaltic liquids generated from a partially depleted lherzolite at 9 kbar pressure. *Nature* **299**, 336–338.

Sen, G. (1985). Experimental determination of pyroxene compositions in the system $CaO–MgO–Al_2O_3–SiO_2$ at 900–1200°C and 10–15 kbar using PbO and H_2O fluxes. *American Mineralogist* **70**, 678–695.

Sigurdsson, I. A., Steinthorsson, S. & Gronvold, K. (2000). Calcium-rich melt inclusions in Cr-spinels from Borgarhraun, northern Iceland. *Earth and Planetary Science Letters* **183**, 15–26.

Slater, J., McKenzie, D., Gronvold, K. & Shimizu, N. (2001). Melt generation and movement beneath Theistareykir, NE Iceland. *Journal of Petrology* **42**, 321–354.

Sours-Page, R., Johnson, K. T. M., Nielsen, R. L. & Karsten, J. L. (1999). Local and regional variation of MORB parent magmas: evidence from melt inclusions from the Endeavour Segment of the Juan de Fuca Ridge. *Contributions to Mineralogy and Petrology* **134**, 342–363.

Takahashi, E. & Kushiro, I. (1983). Melting of a dry peridotite at high pressures and basalt magma genesis. *American Mineralogist* **68**, 859–879.

Walter, M. J. & Presnall, D. C. (1994). Melting behaviour of simplified lherzolite in the system $CaO–MgO–Al_2O_3–Na_2O$ from 7 to 35 kbar. *Journal of Petrology* **35**, 329–359.

Walter, M. J., Sisson, T. W. & Presnall, D. C. (1995). A mass proportion method for calculating melting reaction and application to melting of model upper mantle lherzolite. *Earth and Planetary Science Letters* **135**, 77–90.

Ware, N. G. (1991). Combined energy-dispersive–wavelength-dispersive quantitative electron microprobe analysis. *X-ray Spectrometry* **20**, 73–79.

Witt-Eickschen, G. & Seck, H. A. (1991). Solubility of Ca and Al in orthopyroxene from spinel peridotite: an improved version of an empirical geothermometer. *Contributions to Mineralogy and Petrology* **106**, 431–439.